TR - H - 175

Chaotic Potts spin

Shin ISHII　　*Masaaki SATO*

1995. 11. 24

ATR人間情報通信研究所

〒619-02　京都府相楽郡精華町光台2-2　☎ 0774-95-1011

ATR Human Information Processing Research Laboratories
2-2, Hikaridai, Seika-cho, Soraku-gun, Kyoto 619-02 Japan
Telephone: +81-774-95-1011
Facsimile: +81-774-95-1008

Chaotic Potts spin

Shin Ishii **Masa-aki Sato**

ATR Human Information Processing Research Laboratories

2-2 Hikaridai, Seika-cho, Soraku-gun, Kyoto 619-02, Japan

(TEL) +81-774-95-1069 (FAX) +81-774-95-1008

(E-mail) ishii@hip.atr.co.jp

Abstract

In this paper, first, we show some of the bifurcation properties of Potts mean field theory annealing applied to traveling salesman problems. Due to these bifurcation properties, this approach, in general, produces non-optimal and non-unique solutions. As an alternative approach, we propose a nonequilibrium version of the Potts spin neural network, called Chaotic Potts Spin (CPS). CPS has several parameters, and bifurcation over each parameter is investigated. Next, experimental results are shown comparing CPS with several related approaches. CPS is good at obtaining the optimal solutions for small-scale problems and semi-optimal solutions for relatively large-scale problems. We also describe a modified algorithm in which a heuristic method is employed. This modified algorithm can produce even better CPS solutions.

1 Introduction

There have been many studies on artificial neural network models applied to combinatorial optimization problems. Most famous is the analog Hopfield network (Hopfield & Tank, 1985), which is equivalent to the mean field theory (Peterson & Anderson, 1988) of the Boltzmann machine (Ackley et al., 1985). In the mean field theory (MFT), when the system's temperature is low, the free energy function is nearly equal to the energy function to be minimized. The MFT can be combined with a gradual lowering of the temperature, and the combined algorithm is the MFT annealing algorithm (Bilbro et al., 1989). In all of these approaches, state variables are primarily defined to be unconstrained and independent of each other. Therefore, the constraints of a problem are implemented as soft constraints, namely, the energy function includes the corresponding penalty terms. The above-mentioned approaches are called Ising spin approaches, since each state variable represents binary states.

In TSPs, graph bisection problems, N-Queen problems and so on, neural network representations have a common structure, i.e., for some state variables, their summation must be a constant. Focusing on this property, a Potts spin system (Wu, 1982) was employed in the MFT annealing approach; this is the Potts MFT annealing approach (Peterson & Söderberg, 1989; Van den Bout & Miller, 1989). A Potts spin is a generalization of an Ising spin so as to take more-than-two states. By employing a Potts spin system, some of the soft constraints are treated as hard constraints, namely, they hold automatically. This makes the domain space, where solutions are searched for, smaller than in the Ising spin approaches. As a result, the obtained solutions are much improved. Peterson (1990) showed that the performance of Potts MFT annealing is comparable to simulated annealing (Kirkpatrick et al., 1983) and to some other conventional algorithms even for large-scale problems.

In both Ising spin and Potts spin MFT annealing, during the course of the annealing process, a sequence of bifurcations for minimum solutions occurs. The structure of the bifurcations, which affects the quality of the annealing solution, is dependent on the problem's symmetries (Golubitsky et al., 1988). We (Sato & Ishii, 1995) have investigated MFT bifurcation processes when MFT annealing was applied to traveling salesman problems (TSPs). Without structurally stable symmetries in the problem, one can generically expect only saddle-node bifurcations to occur. However, the free energy function for a TSP has two types of symmetries, i.e., cyclic and reverse symmetries. Due to these symmetries, special types of bifurcations also occur. They are called cyclic symmetry breaking bifurcations and reverse symmetry breaking bifurcations. In TSPs, the unique minimum at high temperature has cyclic and reverse symmetries. In contrast, feasible minima at low temperature, which correspond to Hamilton paths, have no symmetry. Therefore, the symmetric minimum at high temperature bifurcates into equivalent minima with no symmetry or is annihilated at some temperature through bifurcations. It should be noted that new minima are mostly generated by saddle-node bifurcations.

If an annealing solution is annihilated at some temperature and there are more than two distinctive minima at this temperature, whatever minimum is obtained by the MFT annealing is not unique due to the instability at the annihilation point. In fact, the annihilation is quite a typical phenomenon. This implies that the solution of the MFT annealing is not unique in general, even though the procedure is deterministic.

When new minima are generated, their free energy levels are higher than that of the

global minimum at that temperature. However, the free energy levels of some minimum solutions may cross one another as the temperature is lowered. Therefore, the MFT annealing procedure does not always give the optimal solution. As a consequence, the annealing solution in the MFT annealing is, in general, a not-so-bad solution and is not unique.

On the other hand, Nozawa (1992) showed that a chaotic version of the analog Hopfield network can find the optimal solutions of small-scale TSPs nearly 100% of the time. His model is based on a Euler difference equation of the Hopfield network with inhibitory self-loops; this model is equivalent to the Chaotic Neural Network model proposed by Aihara et al. (1990). Euler difference equation systems with self-loops have been known to give chaotic solutions even when their original differential equation systems were giving stable solutions (Yamaguti & Matano, 1979). Although Nozawa's model is good at obtaining the optimal solutions for small-scale problems, it does not give very good solutions for large-scale problems. We guess there are two reasons. One is due to its strong nonequilibrium dynamics. Nozawa employs heuristic methods to suppress some of the nonequilibrium dynamics. However, they are not sufficient to get the optimal solutions for large-scale problems. The other is due to the Ising spins it employs. Since the domain space becomes too large with unconstrained state variables when the problem scale is large, even the chaotic dynamics can not retrieve good solutions.

In this paper, we propose an alternative approach, that is, a nonequilibrium version of the Potts spin neural network, which is called Chaotic Potts Spin (CPS). CPS is based on a Euler difference equation of the continuous-time Potts spin neural network model with inhibitory self-loops. This modification makes the Potts spin neural network into a nonequilibrium dynamical system. Since our CPS employs a Potts spin system, its domain space is smaller than in the Ising spin approaches. Moreover, since it is a nonequilibrium dynamical system, the above-mentioned adverse properties in the annealing algorithms can be overcome.

This paper is organized as follows. In Section 2, we show the bifurcation structures of the Potts MFT annealing. In the Potts MFT annealing, although the above-mentioned adverse properties are much improved in comparison with Ising spin MFT annealing, they are not entirely overcome. In Section 3, we propose our alternative approach, namely, CPS. CPS has several parameters. In Section 4, we investigate bifurcation over each of those parameters. In Section 5, experimental results are shown comparing CPS with several related approaches. CPS is good at obtaining the optimal solutions for small-scale problems and semi-optimal solutions for relatively large-scale problems. In Section 6, we describe a modified algorithm in which a heuristic method is employed. This modified algorithm can produce even better solutions.

2 Potts mean field theory annealing and TSP

2.1 Potts mean field theory

Some of the $\mathcal{NP}$-complete optimization problems can be described as a quadratic energy minimization problem for $(M \times N)$-dimensional Potts spin variables $S_{a,n}(= 0 \text{ or } 1)$:

$$E(\mathbf{S}) = \frac{1}{2} \sum_{a,b=1}^{M} \sum_{n,m=1}^{N} W_{a,n;b,m} S_{a,n} S_{b,m} + \sum_{a=1}^{M} \sum_{n=1}^{N} I_{a,n} S_{a,n}, \tag{2.1}$$

where $W_{a,n;b,m} = W_{b,m;a,n}$ and $\sum_{n=1}^{N} S_{a,n} = 1 \quad (a = 1, ..., M)$ are assumed. $S_{a,n}$ denotes the n-th component of the a-th Potts spin (Wu, 1982). The network consists of M N-state Potts spins. The values of the parameters $\mathbf{W}$ and $\mathbf{I}$ are determined for each problem. By introducing analog variable $V_{a,n} \in [0, 1]$, which represents the probability that the binary variable $S_{a,n}$ takes the value 1, the mean field theory (MFT) free energy function is given by:

$$F(\mathbf{V}) = E(\mathbf{V}) - T \cdot H(\mathbf{V}) \tag{2.2a}$$

$$H(\mathbf{V}) = -\sum_{a,n} V_{a,n} \log V_{a,n} \ . \tag{2.2b}$$

where $H(\mathbf{V})$ is the entropy function, and T is the temperature. The MFT solution of (2.2) is a minimum of the MFT free energy function, where the following stationary condition is satisfied:

$$U_{a,n} = \sum_{b,m} W_{a,n;b,m} V_{b,m} + I_{a,n} \tag{2.3a}$$

$$V_{a,n} = G_n(\mathbf{U}_a) = \frac{\exp(-U_{a,n}/T)}{\sum_m \exp(-U_{a,m}/T)}. \tag{2.3b}$$

Because of (2.3b), the constraints:

$$\sum_{n=1}^{N} V_{a,n} = 1 \qquad (a = 1, ..., M) \tag{2.4}$$

are automatically satisfied. This equation is called Potts MFT equation (Peterson & Söderberg, 1989). The solution of (2.3) can be obtained by using the continuous-time Potts spin model:

$$\tau \frac{dU_{a,n}}{dt} = -U_{a,n} + \sum_{b,m} W_{a,n;b,m} V_{b,m} + I_{a,n} \tag{2.5a}$$

$$V_{a,n} = G_n(\mathbf{U}_a) = \frac{\exp(-U_{a,n}/T)}{\sum_m \exp(-U_{a,m}/T)}, \tag{2.5b}$$

where t denotes continuous-time. This differential equation system globally converges, and the MFT free energy function (2.2) becomes its Lyapunov function that always decreases over time. This proof is briefly described in Appendix A.

The solution of the Potts MFT equation (2.3) can also be obtained by using the asynchronous Potts MFT equation (Peterson & Söderberg, 1989):

$$U_{a,n}(t) = \sum_{b,m} W_{a,n;b,m} V_{b,m}(t-1) + I_{a,n} \tag{2.6a}$$

$$V_{a,n}(t) = G_n(\mathbf{U}_a(t)) \tag{2.6b}$$

$$V_{b,m}(t) = V_{b,m}(t-1) \quad \text{for } b \neq a, \tag{2.6c}$$

where t denotes discrete-time. If we assume

$$W_{a,n;a,m} = 0 \qquad \text{for any } a, n, m, \tag{2.7}$$

(2.6) converges to a local minimum of the free energy function (2.2) (Sato, 1994). Since the system implemented by Peterson and Söderberg (1989) does not satisfy the condition (2.7), their system does not always converge.

At high temperature, the free energy (2.2) is dominated by the entropy term, and there is a unique minimum. At low temperature, the free energy function is nearly equal to the energy function $E(\mathbf{V})$. Therefore, at low temperature, there are local minima of the free energy function (2.2) that correspond to those of the energy function (2.1).

In order to get a good local minimum of the energy function (2.1), an annealing procedure can be used. First, the MFT equation (2.3) is solved for a high temperature value. Then, after a slight lowering of the temperature, the MFT equation is solved again starting from the higher temperature solution. By continuing this process, one can get a low temperature solution. This algorithm is called Potts MFT annealing (Peterson & Söderberg, 1989; Van den Bout & Miller III, 1989). During the course of the temperature lowering, bifurcations occur and new minima are generated. These bifurcations are dependent on the structural stable symmetries in the problem (Golubitsky et al., 1988).

2.2 TSP and symmetries

A Potts spin energy function for an N-city TSP is given as:

$$E(\mathbf{V}) = \frac{1}{2}\sum_{a,b,n=1}^{N} D_{a,b}V_{a,n}(V_{b,n+1}+V_{b,n-1}) + \frac{\alpha}{2}\sum_{n=1}^{N}(\sum_{a=1}^{N}V_{a,n}-1)^2 + \frac{\beta}{2}\sum_{a=1}^{N}\sum_{n\neq m}^{N}V_{a,n}V_{a,m}, \quad (2.8)$$

where $V_{a,n}(a,n=1,...,N)$ represents the probability that the salesman visits city a at the n-th visit, and $D_{a,b}$ denotes the distance between city a and city b. The first and second r.h.s. terms in (2.8) denote the total tour length and the soft constraint that must hold for representing a Hamilton path, respectively. The third term becomes zero and does not affect the free energy when the temperature is low. However, it actually contributes to stabilizing the MFT solutions, because this term partly cancels the inhibitory self-loops.

The energy function (2.8) and the corresponding free energy function are invariant under the N-th order cyclic transformation: $\mathbf{V} \longrightarrow \mathcal{T}_m^{[N]}\mathbf{V}$ $(m=1,...,N-1)$, where $(\mathcal{T}_m^{[N]}\mathbf{V})_{a,n} = V_{a,n+m}$, and the N-th order reverse transformation: $\mathbf{V} \longrightarrow \mathcal{R}_m^{[N]}\mathbf{V}$ $(m=0,1,...N-1)$, where $(\mathcal{R}_m^{[N]}\mathbf{V})_{a,n} = V_{a,m-n}$. Due to these symmetries, a solution of an N-city TSP has $2N$ equivalent representations.

There is a symmetric stationary solution $\mathbf{V}^s$ of the free energy function for any T: $V^s_{a,n} = 1/N$. Since $\mathcal{T}_m^{[N]}\mathbf{V}^s$ and $\mathcal{R}_m^{[N]}\mathbf{V}^s$ coincide with $\mathbf{V}^s$, $\mathbf{V}^s$ is said to have the N-th order cyclic and reverse symmetries. Since the free energy function (2.2) has a unique minimum at high temperature, the unique minimum must be $\mathbf{V}^s$. In contrast, feasible minima at low temperature, which correspond to Hamilton paths, have no symmetry. Therefore, the symmetric minimum $\mathbf{V}^s$ at high temperature bifurcates into equivalent minima with no symmetry or is annihilated at some temperature through bifurcations.

2.3 Bifurcations of Potts MFT annealing

If there is no structurally stable symmetry in the problem, one can generically expect that only saddle-node bifurcations will occur. However, a TSP has the above-mentioned cyclic

and reverse symmetries. Due to them, special types of bifurcations also occur. They are called cyclic symmetry breaking bifurcations and reverse symmetry breaking bifurcations. Which bifurcation type occurs depends on the symmetry of the eigenvector that corresponds to the zero eigenvalue mode of the free energy curvature matrix at the bifurcation point (Sato & Ishii, 1995). For example, when the bifurcation point has the N-th order cyclic symmetry and the eigenvector has no symmetry, a cyclic symmetry breaking bifurcation will occur. Figure 1 shows schematic figures of cyclic symmetry breaking bifurcations, where $N = 5$. Note that in Figure 1(d), the high temperature minimum turns into a saddle-point and disappears (annihilation) at the critical temperature; this is a common observation in Ising spin MFT annealing.

Let us show an example. Figure 2(c) shows a typical bifurcation diagram of a 5-city TSP whose optimal tour is shown in Figure 2(a). The values of $V_{1,i}$ $(i = 1, ..., 5)$ for each minimum are plotted for each temperature. Figure 2(d) shows the corresponding free energy diagram. In Figure 2(c), we can observe a cyclic symmetry breaking bifurcation at $T \approx 0.32$, and a reverse symmetry breaking bifurcation at $T \approx 0.29$. At $T \approx 0.27, 0.21$, and 0.19, we can also observe saddle-node bifurcations, where new minima are generated.

The Potts MFT annealing procedure is a series of the local bifurcations and has the following properties.

- **non-optimality**
  In Figure 2(d), the free energy level of the annealing solution and the newly generated minima that appear at $T \approx 0.27$ cross each other. After the free energy crossing, the annealing solution level becomes higher than the new minima level, and turns into a local minimum. In this case, the Potts MFT annealing fails to obtain the optimal solution, instead producing a semi-optimal solution as shown in Figure 2(b).

- **non-uniqueness**
  When the annealing solution disappears at some temperature, e.g., through a cyclic symmetry breaking bifurcation as shown in Figure 1(d), and there are two or more distinctive minima at this temperature, the annealing may produce non-unique solutions.

The above-mentioned properties are almost the same as in the Ising spin MFT annealing case. However, there are some differences. For instance, in Ising spin MFT annealing, since the disappearance of the annealing solution is quite a typical phenomenon, the annealing procedure results in non-unique solutions in general. Figure 2(e) shows the bifurcation diagram of the Ising spin MFT annealing for the same problem, where the annealing solution disappears at $T \approx 0.475$. On the other hand, in Potts spin MFT annealing, the disappearance is less typical.

In a relatively small-scale problem, in particular, the unique minimum at high temperature tends to bifurcate into $2N$ equivalent minima with no symmetry through one or more cyclic symmetry breaking bifurcations and a reverse symmetry breaking bifurcation. These minima represent a valid Hamilton path, although this may not signify the optimal tour. In such a case, the annealing procedure results in a unique solution. We guess that this quantitative difference is due to the soft constraint terms in the energy function. Actually, if we remove soft constraint terms from the Ising spin MFT energy function, the disappearance seldom occurs, while most of the obtained solutions fail to be valid Hamilton paths.

In the Potts MFT annealing, we can reduce the soft constraint terms; this prevents the annealing solution from being annihilated and hence reduces the non-uniqueness. This is regarded as one reason why Potts MFT annealing can obtain much better solutions than Ising spin MFT annealing. This improvement becomes more prominent, if we design an energy function without soft constraint terms (Ishii & Sato, 1995).

Accordingly, it can be said that the Potts MFT annealing results are, in general, non-optimal and non-unique, although the non-uniqueness is much improved in comparison with Ising spin MFT annealing. To overcome these adverse properties, we propose an alternative approach.

3 Chaotic Potts Spin

3.1 Model description

If we apply a Euler method to the continuous-time Potts spin model (2.5), a difference equation is obtained:

$$U_{a,n}(t) = kU_{a,n}(t-1) + (1-k)\left(\sum_{b,m} W_{a,n;b,m}V_{b,m}(t-1) + I_{a,n}\right) \tag{3.1a}$$

$$V_{a,n}(t) = G_n(\mathbf{U}_a(t)), \tag{3.1b}$$

where $k = 1 - \delta t/\tau$, and δt denotes the time interval. As shown in Section 2.1, the original differential equation system (2.5) always converges to a local minimum of the free energy function (2.2). However, if we choose W to be $W_{a,n;a,n} > 0$, (3.1) often exhibits chaotic solutions. We thus call the difference equation system (3.1) Chaotic Potts Spin (CPS).

Let us apply CPS to the TSP energy function (2.8). CPS for a TSP is defined as:

$$\begin{aligned} U_{a,n}(t) = kU_{a,n}(t-1) &+ \sum_b D'_{a,b}(V_{b,(n+1)}(t-1) + V_{b,(n-1)}(t-1)) \\ &+ \alpha' \sum_b V_{b,n}(t-1) - \beta' V_{a,n}(t-1) \end{aligned} \tag{3.2a}$$

$$V_{a,n}(t) = G_n(\mathbf{U}_a(t)), \tag{3.2b}$$

where $D'_{a,b} = (1-k)D_{a,b}$, $\alpha' = (1-k)\alpha$, and $\beta' = (1-k)\beta$. Network parameters, $\mathbf{W}$ and $\mathbf{I}$, are determined as:

$$W_{a,n;b,m} = D_{a,b}(\delta_{n,(m-1)} + \delta_{n,(m+1)}) + \alpha\delta_{n,m} - \beta\delta_{a,b}\delta_{n,m} \tag{3.3a}$$

$$I_{a,n} = 0, \tag{3.3b}$$

where δ is Kronecker's delta. To make the self-loops positive, $\alpha > \beta$.

3.2 Algorithm

There are several algorithms to implement the CPS equation (3.1). The following is a basic asynchronous algorithm, where state variables are updated in a fixed order.

[Basic algorithm]

1. Set $\mathbf{U}$ at a random initial state.
2. For $sweep = 1, ..., \#sweep$, do as follows:
   (a) For $a = 1, ...N$, do as follows:
      i. Update the internal states $U_{a,n}$ $(n = 1, ...N)$ corresponding to the a-th spin by (3.1a).
      ii. Update the a-th spin variables $V_{a,n}$ $(n = 1, ...N)$ by (3.1b).
   (b) Binarize the state variables $\mathbf{V}$ and get $\mathbf{S}$. If $\mathbf{S}$ corresponds to a valid Hamilton path, memorize it.
3. Select the best tour among the memorized tours.

During a single "sweep", all of the variables are updated once and only once. In Step 2(a), we choose to update spins in a fixed order, although the order itself is not very important. In the asynchronous Potts MFT equation (2.6), in contrast, the spin updating order is sometimes very important, because it determines which local minimum is searched for. In Step 2(b), we adopt the following binarizing scheme: 1 if $V_{a,n}$ is the maximum value among $V_{a,*}$ and 0 otherwise. This is the most reasonable scheme because V_a originally denotes a single Potts spin.

There are some other algorithms. One is an asynchronous updating algorithm where updating spins are chosen in random order. Another is a synchronous updating algorithm. These three algorithms differ in terms of stability. Therefore, their optimal parameter values also differ. According to our experiments, the synchronous algorithm is not good, because it tends to become two-cycle periodic solutions, and both of the states do not correspond to any valid Hamilton paths. In what follows, therefore, we deal with two algorithms, namely, a fixed-order asynchronous algorithm and a random-order asynchronous algorithm.

Figure 3(b) shows the process of a fixed-order CPS algorithm applied to the famous 10-city problem (Hopfield & Tank, 1985) whose optimal tour is shown in Figure 3(a). The parameters are $k = 0.7, \alpha' = 0.8, \beta' = 0.0$ and $T = 0.05$. Each circle denotes the obtained tour at each sweep. Where no circle is plotted, no valid tour was obtained at that sweep. Figures 3(c) and 3(d) show the time-series of the variable $V_{1,1}$ and the energy function $E(\mathbf{V})$ (2.8), respectively. Each variable moves chaotically, and the optimal and semi-optimal solutions are retrieved over time. We can observe a correspondence between Figures 3(b) and 3(d). For example, at $sweep \approx 450$, the energy function $E(\mathbf{V})$ is relatively high for a while as shown in Figure 3(d), and no solution is obtained at that period in Figure 3(b).

4 Bifurcations of CPS

Let us investigate the CPS bifurcation over each parameter. The temperature T, the inhibitory self-loops $W_{a,n;a,n}$ and the time interval parameter k are bifurcation parameters that determine the stability of (3.1). In this entire section, the 5-city TSP shown in Figure 2 is used.

4.1 Fixed-order algorithm

In this part, we investigate the bifurcations when the fixed-order asynchronous updating algorithm is employed. The basic parameter values are: $k = 0.7, \alpha' = 0.8, \beta' = 0.0$, and $T = 0.05$, which are experimentally good parameter values. The CPS bifurcation over each of these parameters is investigated.

4.1.1 Bifurcation over temperature

Figure 4(a) shows a bifurcation diagram over temperature T, where values of a single variable $V_{1,1}$ at $sweep = 100001 \sim 100500$ are plotted at each temperature. The other parameters are fixed at $k = 0.7, \alpha' = 0.8$, and $\beta' = 0.0$. At each temperature, the system's initial state was set near the fixed-point at high temperature, i.e., $V_{a,n}(0) = 1/N +$ small-rand.

For $T > 0.10416...$, the system converges to a fixed-point attractor, and for $T < 0.10416...$, the system does not converge. When the system converges, the solution is a local minimum of the free energy function (2.2), and the bifurcation structures are the same as those in the Potts MFT annealing described in Section 2.3. For $T > 0.12$, there is a unique symmetric minimum and a cyclic symmetry breaking bifurcation occurs at $T \approx 0.12$. The bifurcated minima have a first order reverse symmetry.

Figure 4(b) shows a more detailed bifurcation diagram. At $T = 0.10416...$, a period-doubling bifurcation occurs to break the first order reverse symmetry. Below the critical temperature, the system oscillates in two cycles. At $T = 0.10335...$, the two-cycle periodic attractor changes into a more complex attractor. Figure 5(a1) shows the frequency spectra for $sweep = 100001 \sim 110000$ at $T = 0.1020$, where two independent frequencies are observed. The first frequency is 5000, which represents a two-cycle periodicity, and the second frequency can be estimated at about 224. Figure 5(a2) shows the phase diagram at the temperature, where $(V_{1,1}(s-1), V_{1,1}(s))$ $(s = 100001 \sim 110000)$ is plotted. s denotes the sweep. In this figure, two loops are observed. The dynamical system alternately visits the two loops, which corresponds to the first frequency, and it traverses each loop, which corresponds to the second frequency. Since the loops are continuous, the second frequency should be an irrational number. At $T = 0.1020$, the attractor is thus found to be a quasi-periodic attractor. At $T \approx 0.1018$, a period-doubling bifurcation occurs on the second frequency. Figure 5(b1) shows that the second frequency has turned in half at $T = 0.1015$. Figure 5(b2) is the corresponding phase diagram. Figures 5(c), 5(d) and 5(e) are the frequency spectra diagrams and the phase diagrams at $T = 0.1010, 0.1005$, and 0.1000, respectively; they indicate that the period-doublings continue to occur on the second frequency into chaos. As Figures 5(f1) and 5(f2) show, at $T = 0.0970$, the system takes chaotic orbits. However, at $T = 0.0940$, the system again takes a periodic orbit, as Figures 5(g1) and 5(g2) show. This region is a periodic window, and the periodicity is 70 cycles in this case. On the orbit, after 14 sweeps, the system visits a state that is equivalent but transformed by a fifth order cyclic transformation to the starting state, i.e., $\mathbf{V}(s+14) = \mathcal{T}_1^{[5]}\mathbf{V}(s)$. Thus, the 70-cycle periodic orbit visits 14 distinct states. It does not visit the state transformed by the fifth order reverse transformation. Some of these 14 states represent valid Hamilton paths, while the others do not. When the temperature is lower than in the periodic window, the system again takes chaotic orbits as Figures 5(h1) and 5(h2) show. To implement the algorithm, we

use a temperature value belonging to this chaotic region, e.g., $T = 0.05$.

As shown above, the system takes various types of attractors. Although which type of attractor it takes depends on the parameter values and also on the problem itself, three regions can be observed. In the first region, i.e., at high temperature, the system converges. In the second region, as the temperature decreases, the system's attractor becomes more complex toward chaos through the period-doubling route. In the third region, the system takes chaotic orbits, although there exist many periodic window subregions in it. In the example above, if we plot the bifurcation diagram in more detail, more periodic windows can be observed.

4.1.2 Time-interval and self-loop

Figure 6(a) shows a bifurcation diagram over the time interval parameter k, where $\alpha' = 2.7(1-k), \beta' = 0.0$, and $T = 0.05$. The other experimental conditions are the same as in the previous experiment. In Figure 6(a), various types of attractors can be observed. For large k, i.e., $k > 0.9$, the algorithm is close to the continuous-time model (2.5), and the system converges. When k is small, the system is similar to the Potts MFT equation (2.6) with inhibitory self-loops, and it does not converge in most cases. When k is smaller than in the converging region, the system takes quasi-periodic attractors. Figures 6(b) and 6(c) are the frequency spectra diagram and the phase diagram at $k = 0.89$, respectively. If k is smaller than in the quasi-periodic region, the system takes a 6-cycle periodic orbit. This periodic orbit visits six distinct states and these states are not transformed to each other by the fifth order cyclic transformation. When k is further decreased, the system takes chaotic orbits. Here, some other small regions can also be observed as Figure 6(a) shows. We set the time interval parameter value at 0.7, which is in the chaotic region.

Figure 7(a) shows a bifurcation diagram over the parameter β', where $k = 0.7, \alpha' = 0.8$, and $T = 0.05$. When $\beta' = 0.8$, the system is equivalent to the Potts MFT equation (2.6) with no self-loops and it converges. Therefore, with a relatively large β' value, the system converges. However, as β' becomes small, the inhibitory self-loops become large, and the system no longer converges. In this case, the attractors change from a fixed-point to chaotic orbits very rapidly. For $\beta' > 0.251$, the system converges to a fixed-point. At $\beta' = 0.25098$, the system takes a quasi-periodic attractor as shown by the phase diagram in Figure 7(b). At $\beta' = 0.25097$, the quasi-periodicity changes to an 8-cycle periodicity as shown in Figure 7(c). This periodicity rapidly increases through period-doublings into chaos as β' becomes small. Figures 7(d) and 7(e) show the phase diagrams at $\beta' = 0.25090$ and 0.25088, respectively. We set the self-loop parameter β' at 0.0, which is in the chaotic region.

4.2 Random-order algorithm

In this part, we investigate the bifurcations when the random-order asynchronous updating algorithm is employed. Since the algorithm is a probablistic dynamical system, it is very difficult to analyze its bifurcations. The basic parameter values are: $k = 0.7, \alpha' = 0.22, \beta' = 0.04$, and $T = 0.02$, which are experimentally good parameter values.

4.2.1 Bifurcation over temperature

Figure 8(a) shows a bifurcation diagram over temperature T, where the other parameters are fixed at $k = 0.7, \alpha' = 0.22$, and $\beta' = 0.04$. At each temperature, 200 sets of initial states are prepared and each $V_{1,1}(s)$ value for $sweep = 5001 \sim 5100$ is plotted. For $T > 0.04$, the random-order algorithm converges. Since 200 initial states are prepared for each temperature, several solutions are observed in Figure 8(a). If we fix the initial state at every temperature, only one cascade is observed for $T > 0.04$. Figure 8(b) shows the simulation result of the maximum Lyapunov exponent (MLE) against temperature T. The MLE disturbance observed in $0.075 > T > 0.045$ is due to the co-existence of two distinct minima as shown in Figure 8(a). As in the case of the fixed-order algorithm, in the parametric region where the system converges, the bifurcation structures are the same as in the Potts MFT annealing case. For $T > 0.15$, there is a unique symmetric minimum and we can observe a cyclic symmetry breaking bifurcation at $T \approx 0.15$ and a saddle-node bifurcation at $T \approx 0.07$. On the other hand, for $T < 0.04$, MLE is positive and the system becomes chaotic.

Let us further discuss this stability change. Figure 9 shows the phase diagrams for various temperature values. At $T = 0.036$, the system no longer converges, but its unstable motion is almost localized and the orbit tends to remain in the vicinity of the initial state. As the temperature decreases, the unstable motion rapidly becomes large, and each state variable becomes able to switch its value from near 0 to near 1. This value switch occurs in an intermittent manner. Figure 10 shows the value distribution of a single variable $V_{1,1}$ at $T = 0.033$. Note that in TSPs, each binary variable is assigned 1 with the probability of $1/N$ and 0 with $(1 - 1/N)$ in order to properly represent valid Hamilton paths. Figure 10 implies that the random-order algorithm's dynamics give a good value distribution on each variable.

Figures 11 shows solutions obtained by the algorithm, where $T = 0.025$. Since the second best solution shown in Figure 2(b) is the MFT annealing solution, it is the dominant solution in CPS. The above-mentioned intermittent switch changes each variable's value between 0 and 1, which enables the random-order algorithm to retrieve over possible solutions. Hence, the algorithm works well as a solver of combinatorial optimization problems.

Our experiments show that the quality of the obtained solutions is significantly dependent on the temperature value.

4.2.2 Time-interval and self-loop

Figure 12(a) shows a bifurcation diagram over the time interval parameter k, where $\alpha' = 0.72(1 - k), \beta' = 0.14(1 - k)$, and $T = 0.02$. The other conditions are the same as in the previous experiment. Figure 12(b) is the corresponding MLE diagram. When k is close to 1, which implies that the algorithm is nearly equal to the continuous-time model (2.5), the MLE is negative and the system converges. When k is not close to 0, however, the MLE is positive and the system no longer converges and becomes chaotic. Figures 12(c) and 12(d) show the phase diagrams with $k = 0.78$ and 0.73, respectively.

Figure 13(a) shows a bifurcation diagram over the parameter β', where $k = 0.7, \alpha' = 0.22$, and $T = 0.02$. Figure 13(b) is the corresponding MLE diagram. As β' becomes large, the

positive self-loops $W_{a,n;a,n} = (\alpha' - \beta')/(1-k)$ become small, which implies that the algorithm is similar to the asynchronous MFT equation (2.6). Then, the MLE is negative and the system converges. Figures 13(c) and 13(d) show the phase diagrams with $\beta' = 0.08$ and 0.06, respectively.

According to our experiment, the ability of the random-order algorithm is not significantly dependent on these two parameters, while it is sensitive to the temperature T.

5 Experiments

Let us show experimental results comparing CPS with several related approaches. In what follows, we employ the random-order algorithm, because our experiments show that the random-order algorithm can obtain slightly better solutions than the fixed-order algorithm.

In Table 1, we compare CPS with Potts MFT annealing (PMA) (Peterson & Söderberg, 1989), the Chaotic Neural Network (CNN) (Nozawa, 1992), and Ising spin MFT annealing (MFA) (Bilbro et al., 1989). Like with CPS, a result of CNN is the best tour it finds during the entire sweeps. We prepared five testbeds for evaluation: 10-city, 20-city, 30-city, 40-city, and 50-city TSPs. Each testbed had 100 sets of city allocations randomly generated in a unit square. Some normalizations were also done. A brief algorithm description and the employed parameter values are given in Appendix B. In each column of Table 1, the upper number and the lower number denote the number of valid tours obtained by each approach and the averaged tour length for all valid tours obtained, respectively.

In the Potts spin approaches, i.e., CPS and PMA, the possible solutions will be on the N dimensional hypergrids whose number is N^N. On the other hand, in the Ising spin approaches, i.e., CNN and MFA, the possible solutions will be on the $N \times N$ dimensional hypercube vertices whose number is 2^{N^2}. Therefore, the Potts spin approaches have a greater advantage with respect to the domain space to be searched. Note that MFA is a better algorithm than the analog Hopfield network (Hopfield & Tank, 1985) that is equivalent to MFT with no annealing mechanism.

As already mentioned, PMA definitely fails to obtain the optimal solution when the free energy crossing occurs. Even in such a case, CPS, which is a nonequilibrium dynamical system, has the possibility of finding the optimal solution. Actually, for 10-city TSPs, CPS can obtain the optimal solution 98% of the time. This merit is also true for CNN compared with MFA. However, when the number of cities becomes large, even CPS cannot find the optimal solution, because the space to be searched becomes too large. In CPS, with its nonequilibrium property, even if most parts of a solution are good, some other parts can be somewhat random. Therefore, with a relatively large number of cities, CPS becomes inferior to PMA. Still, CPS can always obtain valid tours for every problem, whereas PMA sometimes fails to obtain valid tours. Accordingly, our CPS approach is good at obtaining the optimal solutions for small-scale problems and semi-optimal solutions for relatively large-scale problems.

The basic CPS algorithm does not employ any annealing procedure and the CPS results are sensitive to the temperature T, which is one of the bifurcation parameters. Although the best temperature value varies according to the city allocation, we fixed it in the above experiment for practical reasons. If we tune the temperature for each problem, CPS's ability

can be improved. This tuning is possible by checking the stability of solutions with an annealing-like procedure.

Table 1 In each column, the upper number and the lower number denote the number of valid tours and the averaged tour length for all valid tours obtained, respectively. For example, in the 20-city PMA case, for 85 sets of city allocations out of 100 sets, valid Hamilton paths were obtained and their averaged tour length was 4.325. In this case, the failed results, i.e., 15 sets, were not included in the averaged tour length.

	10	20	30	40	50
CPS	100	100	100	100	100
	3.459	4.318	5.252	5.967	6.940
PMA	82	85	96	94	86
	3.467	4.325	5.167	5.602	6.185
CNN	90	97	96	96	92
	3.578	4.635	5.778	6.755	7.603
MFA	100	96	98	91	88
	3.591	4.695	5.861	6.640	7.313

6 CPS with local heuristics

In our CPS approach, a solution tends to have some good parts and some bad/random parts in it; this is due to its nonequilibrium dynamics. To improve the obtained solutions, a local optimization method can be used. We chose the 2opt algorithm (Lin & Kernighan, 1973) as a local optimization method. The 2opt algorithm removes all crossing parts in a tour. The basic 2opt algorithm is shown in Appendix C.

[Modified random-order algorithm]

1. Set **U** at a random initial state.
2. For $sweep = 1, ..., \#sweep$, do as follows:
   (a) Randomly select a Potts spin index a $(a = 1, ...N)$ and do as follows:
      i. Update the internal states $U_{a,n}$ $(n = 1, ...N)$ corresponding to the a-th spin by (3.1a).
      ii. Update the a-th spin variables $V_{a,n}$ $(n = 1, ..., N)$ by (3.1b).
   (b) If every spin index is selected once and only once, go to Step 2(c). Otherwise, go to Step 2(a).
   (c) Binarize the state variables **V** and get **S**. If **S** corresponds to a valid Hamilton path, go to Step 2(d). Otherwise, proceed to the next sweep.
   (d) Apply 2opt to **S**, and memorize the result.
3. Select the best tour among the memorized tours.

Every time a solution is obtained by CPS, it is improved by the 2opt. The result of the modified CPS is the best solution among the improved solutions. Although it is known that the 2opt heuristic takes an exponential-order computational time in the worst cases, this modification does not affect the processing time. Since the initial state of each 2opt procedure is close to a good solution, it needs only a negligible processing time.

Table 2 shows experimental results. For comparison, the fourth column gives Potts MFT annealing results improved by the 2opt. The averaged tour length in "PMA" and "PMA+2opt" involves only the valid tours they obtained. If the lengths of "CPS" and "CPS+2opt" are averaged over the same allocations, the results of the CPS approaches become slightly better. The fifth column gives the result of a single 2opt.

Table 2 The averaged tour length. In the basic and modified CPS cases, the averaged tour length is for 100 sets, and in the PMA cases, it is averaged over sets that result in valid Hamilton paths (the numbers are in **Table 1**).

	CPS	CPS+2opt	PMA	PMA+2opt	2opt
10	3.459	3.458	3.467	3.460	3.480
20	4.318	4.228	4.325	4.244	4.333
30	5.252	4.943	5.176	5.029	5.100
40	5.967	5.440	5.602	5.530	5.652
50	6.940	5.941	6.185	6.072	6.226

The ability of the modified CPS is better than that of Potts MFT annealing, and the modified CPS can actually obtain the optimal solution for every 10-city TSP and almost every 20-city TSP. On the other hand, solutions of Potts MFT annealing cannot be similarly improved by the 2opt.

7 Conclusion

The MFT annealing approaches, namely, Ising spin MFT annealing and Potts spin MFT annealing, are very powerful approaches for combinatorial optimization problems. However, due to their bifurcation properties, they may fail to obtain the optimal solution even for a small-scale problem.

As an alternative approach, we proposed a nonequilibrium dynamical system called Chaotic Potts Spin (CPS). Since our CPS employs a Potts spin system, its domain space is smaller than in the Ising spin approaches. Moreover, since it is a nonequilibrium dynamical system, the above-mentioned limitations in the annealing algorithms do not matter.

CPS has several parameters, which determine the stability of the dynamics. We investigated the CPS bifurcations for those parameters, and found period-doubling routes toward chaos.

CPS can solve small-scale problems almost 100% of the time. For relatively large-scale problems, however, CPS is inferior to Potts MFT annealing, while it can obtain semi-optimal solutions for these problems. CPS becomes inferior because, with its nonequilibrium dynamics, some random parts remain in almost every solution it obtains. To deal with this problem,

we proposed a CPS combined with local optimization heuristics, namely, the 2opt algorithm. With this modification, CPS can obtain better solutions than Potts MFT annealing.

CPS is a fast algorithm. Actually, in the experiments described in this paper, CPS was found to be faster than Potts MFT annealing, the Chaotic Neural Network and Ising spin MFT annealing. Moreover, after modifying the Potts neural network hardware (Urahama and Ueno, 1993), it is possible to implement the CPS algorithm into a new hardware configuration. In fact, the implementation of an annealing algorithm is considered to be more difficult; our computer experiments have shown that the annealing procedure is quite sensitive to its precision, and this is a weak point of any hardware implementation.

References

[1] Ackley, D. H., Hinton, G. E., and Sejnowski, T. J. (1985). A learning algorithm for Boltzmann machines. *Cognitive Science*, **9**, 147-169.

[2] Aihara, K., Takabe, T., and Toyoda, M. (1990). Chaotic neural networks. *Physics Letters A*, **144**, 333-340.

[3] Bilbro, G., Mann, R., Miller, T. K., Sydner, W. E., Van den Bout, D. E., and White, M. (1989). Optimization by mean field annealing. In *Advances in Neural Information Processing Systems I* (Denver 1988), ed. D. S. Touretzky, 91-98. San Mateo: Morgan Kaufmann.

[4] Golubitsky, M., Stewart, I., and Schaeffer, D. G. (1988). *Singularities and groups in bifurcation theory, Volume II*, Springer-Verlag (New York).

[5] Hopfield, J. J. (1984). Neurons with graded responses have collective computational properties like those of two-state neurons. *Proceedings of the National Academy of Science USA*, **81**, 3088-3092.

[6] Hopfield, J. J., and Tank, D. W. (1985). "Neural" computations of decisions in optimization problems. *Biological Cybernetics*, **52**, 141-152.

[7] Ishii, S., and Sato, M. (1995). Doubly constrained network model for combinatorial optimization problems. *Proceedings of 1995 International Symposium on Nonlinear Theory and its Applications* (Las Vegas 1995).

[8] Kirkpatrick, S., Gelatt, C. D., and Vecchi, M. P. (1983). Optimization by simulated annealing. *Science*, **220**, 671-680.

[9] Lin, S., and Kernighan, B. W. (1973). An efficient heuristic algorithm for the traveling salesman problem. *Operations Research*, **21**, 498-516.

[10] Nozawa, H. (1992). A neural network model as a globally coupled map and applications based on chaos. *CHAOS*, **2**, 377-386.

[11] Peterson, C., and Anderson, J. R. (1988). Neural networks and NP-complete optimization problems: A performance study on the graph bisection problem. *Complex Systems*, **2**, 59-89.

[12] Peterson, C., and Söderberg, B.(1989). A new method for mapping optimization problems onto neural networks. *International Journal of Neural Systems*, **1**, 3-22.

[13] Peterson, C. (1990). Parallel distributed approaches to combinatorial optimization: benchmark studies on traveling salesman problem. *Neural Computation*, **2**, 261-269.

[14] Sato, M. (1994). The asynchronous MFT equation converges faster than the Hopfield network. *ATR Technical Report*, **TR-H-089**.

[15] Sato, M., and Ishii, S. (1995). Bifurcations in mean field theory annealing. *ATR Technical Report*, **TR-H-167**.

[16] Urahama, K., and Ueno, S-I. (1993). A gradient system solution to Potts mean field equations and its electronic implementation. *International Journal of Neural Systems*, **4**, 27-34.

[17] Van den Bout, D. E., and Miller III, T. K. (1989). Improving the performance of the Hopfield-Tank neural network through normalization and annealing. *Biological Cybernetics*, **62**, 129-139.

[18] Wu, F. Y. (1982). The Potts model. *Reviews of Modern Physics*, **54**, 235-268.

[19] Yamaguti, M., and Matano, H. (1979). Euler's finite difference scheme and chaos. *Proceedings of the Japan Academy. Series A*, **55**, 78-80.

Appendix A

In this appendix section, we briefly prove the global convergence of the differential equation system (2.5). First, the let us define variables Q_a as:

$$Q_a = T(1 - \log \sum_m \exp(-U_{a,m}/T)). \tag{A.1}$$

From (2.5b) and (A.1),

$$Q_a = U_{a,n} + T(\log V_{a,n} + 1) \tag{A.2}$$

holds. From (2.2), (2.5a), and (A.2),

$$\frac{\partial F}{\partial V_{a,n}} = \tau \frac{dU_{a,n}}{dt} + Q_a \tag{A.3}$$

holds. Then, the time derivative of the free energy (2.2) is given by:

$$\begin{aligned} \frac{dF}{dt} &= \sum_{a,n} \left(\frac{\partial F}{\partial V_{a,n}} \right) \left(\frac{dV_{a,n}}{dt} \right) \\ &= -\tau T \sum_{a,n} \frac{1}{V_{a,n}} \left(\frac{dV_{a,n}}{dt} \right)^2 + \sum_a \left(\tau \frac{dQ_a}{dt} + Q_a \right) \sum_n \frac{dV_{a,n}}{dt}. \end{aligned} \tag{A.4}$$

Here, the time derivative of (A.2) is used. From (2.4), $\sum_n dV_{a,n}/dt = 0$. Therefore,

$$\frac{dF}{dt} \leq 0 \tag{A.5}$$

holds, which means that the dynamical system (2.5) globally converges to a local minimum of the free energy function (2.2).

Appendix B

In this appendix section, we briefly describe the algorithms and parameter values of CPS, Potts MFT annealing, the Chaotic Neural Network, and Ising spin MFT annealing.

Table A1 shows the parameter values for the random-order CPS algorithm, which are used in the experiments in Sections 5 and 6.

Table A1 Parameters for CPS

#city	α'	β'	k	T	#sweep
10	0.24	0.05	0.7	0.013	1000
20	0.27			0.010	
30	0.30			0.009	1500
40	0.32	0.06		0.007	2000
50	0.33	0.07		0.006	

Table A2 show the parameter values for Potts MFT annealing. In Potts MFT annealing, each MFT solution is obtained by employing the asynchronous MFT equation (2.6) until $\mathbf{V}$ converges. The convergence is determined when $\delta\mathbf{V}$ in a round becomes smaller than 10^{-3}. In Table A2, T_{init} and δT denote the starting temperature and the temperature lowering step of the annealing procedure. The annealing procedure is terminated when the state is regarded as representing a valid Hamilton path, or the temperature reaches a very low value.

Table A2 Parameters for Potts MFT annealing

#city	α	β	T_{init}	δT	$\delta\mathbf{V}$
10	1.0	0.8	0.40	0.001	10^{-3}
20			0.35		
30			0.30		
40		0.5	0.25		
50			0.22	0.002	

The Chaotic Neural Network (CNN) model is a dynamical system defined as:

$$U_{a,n}(t+1) = kU_{a,n}(t) - \alpha V_{a,n}(t) + (1-k)\left(\sum_{b,m} W_{a,n;b,m}V_{b,m}(t) + I_{a,n}\right) \quad \text{(A.6a)}$$

$$V_{a,n}(t+1) = F(U_{a,n}(t+1)) = \frac{1}{1+e^{-U_{a,n}(t+1)/T}}. \quad \text{(A.6b)}$$

When applying CNN to TSPs, network parameters are determined as:

$$W_{a,n;b,m} = A\left(\delta_{a,b}(1-\delta_{n,m}) + \delta_{n,m}(1-\delta_{a,b})\right) + D_{a,b}(\delta_{n,(m+1)} + \delta_{n,(m-1)}) \quad \text{(A.7a)}$$

$$I_{a,n} = R \times A. \quad \text{(A.7b)}$$

The detailed algorithm is similar to CPS. However, in CNN, there must be a technique. Since the chaotic motion of CNN is too strong, we must average each of the variable values for some period to extract a binary representation from CNN (Nozawa, 1992). We also adopted this technique in the experiment in Section 5, and the period was determined as 20 sweeps. The parameter values were independent of the problem scale and determined as: $k = 0.7, A = 1.0, R = 0.77, \alpha = 0.35$, and $T = 0.007$. *#sweep*'s are the same as in CPS.

Asynchronous Ising spin MFT annealing is a dynamical system solving the following equation asynchronously, i.e., unitwisely:

$$U_{a,n}(t+1) = \sum_{b,m} W_{a,n;b,m}V_{b,m}(t) + I_{a,n} \quad \text{(A.8a)}$$

$$V_{a,n}(t+1) = F(U_{a,n}(t+1)), \quad \text{(A.8b)}$$

where

$$W_{a,n;b,m} = A\left(\delta_{a,b}(1-\delta_{n,m}) + \delta_{n,m}(1-\delta_{a,b})\right) + D_{a,b}(\delta_{n,(m+1)} + \delta_{n,(m-1)}) \quad \text{(A.9a)}$$

$$I_{a,n} = 2A. \quad \text{(A.9b)}$$

The parameter values are shown in Table A3. Convergence of the MFT equation is checked by $\delta \mathbf{V}$. T_{init} and δT denote the starting temperature and the temperature lowering step of the annealing procedure. The annealing procedure is terminated when the state is regarded as representing a valid Hamilton path, or the temperature reaches a very low value.

Table A3 Parameters for Ising spin MFT annealing

#city	A	T_{init}	δT	$\delta \mathbf{V}$
10	1.5	1.5	0.001	10^{-6}
20	1.6			
30				
40				
50	1.5	0.8		

Appendix C

The following is the pseudo code of the most basic 2opt algorithm. The function "NextCity" returns the next city of the input city on the present tour. The function "FlipCities(A,B,X,Y)" disconnects pass AB and pass XY on the present tour and reconnects pass AX and pass BY. In this reconnection, the sequence between B and X (or, between Y and A) is reversed in its order. D(A,B) is the distance between A and B.

```
TwoOpt() {
MakeRandomInitialTour();
start:
  for all city A on the tour {
    B = NextCity(A);
      for all city X excluding the city A {
        Y = NextCity(X);
        if(D(A,B)+D(X,Y)-D(A,X)-D(B,Y) > 0) {
           FlipCities(A,B,X,Y);
           goto start;
        }
     }
  }
}
```

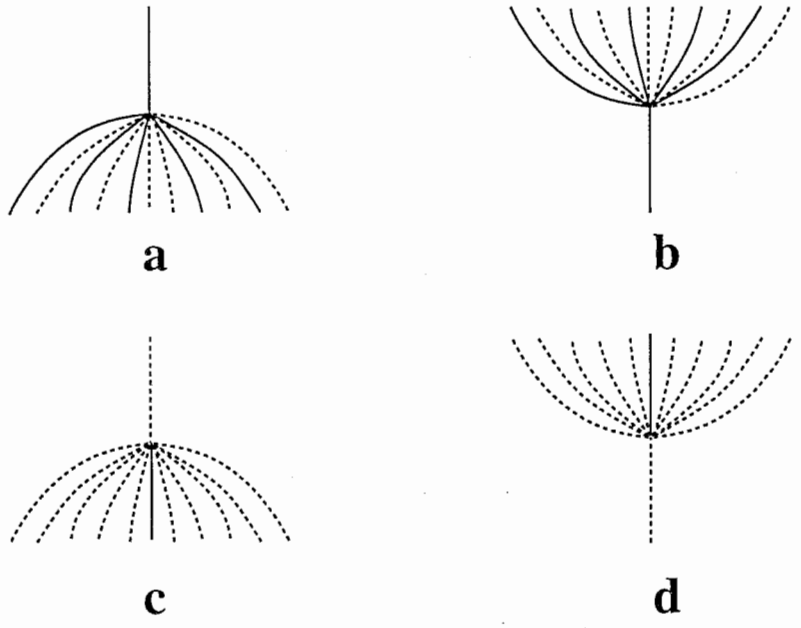

Figure 1

Schematic figures of cyclic symmetry breaking bifurcations, where $N = 5$. The abscissa denotes the value of a state variable, and the ordinate denotes the temperature. The upper side of each figure denotes higher temperature. The solid line and dotted line denote a stable stationary point (minimum) and an unstable stationary point (saddle point), respectively. The straight line and curved line denote a stationary point with the 5th order cyclic symmetry, and a stationary point without the cyclic symmetry, respectively. (a) A minimum with the 5th order cyclic symmetry bifurcates into a saddle-point with the 5th order cyclic symmetry, five minima without the cyclic symmetry, and five saddle-points without the cyclic symmetry.

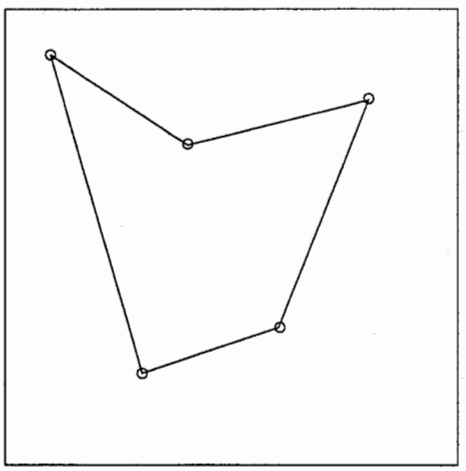

Figure 2(a)

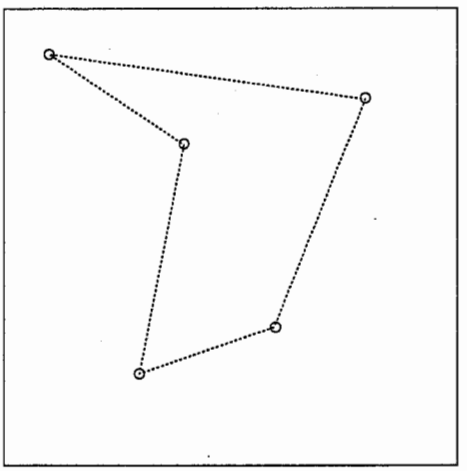

Figure 2(b)

Sample 5-city problem. (a) The optimal tour. (b) The second best tour.

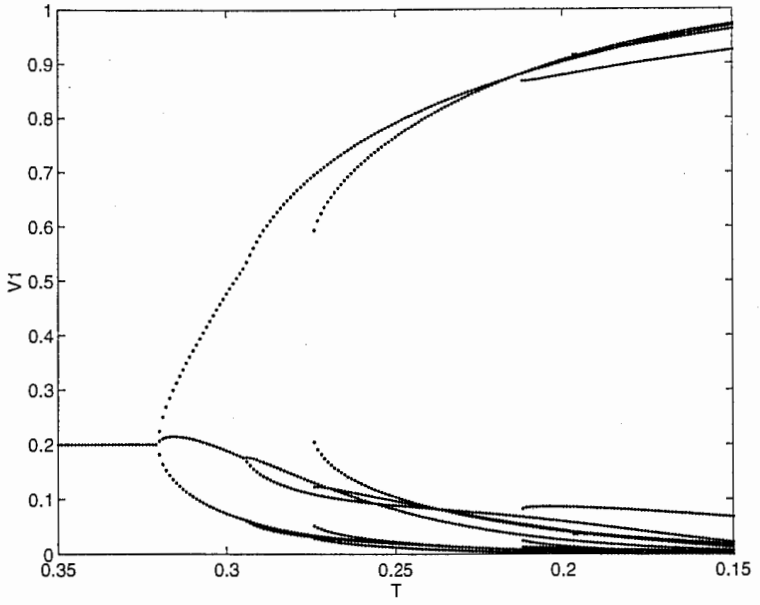

Figure 2(c)

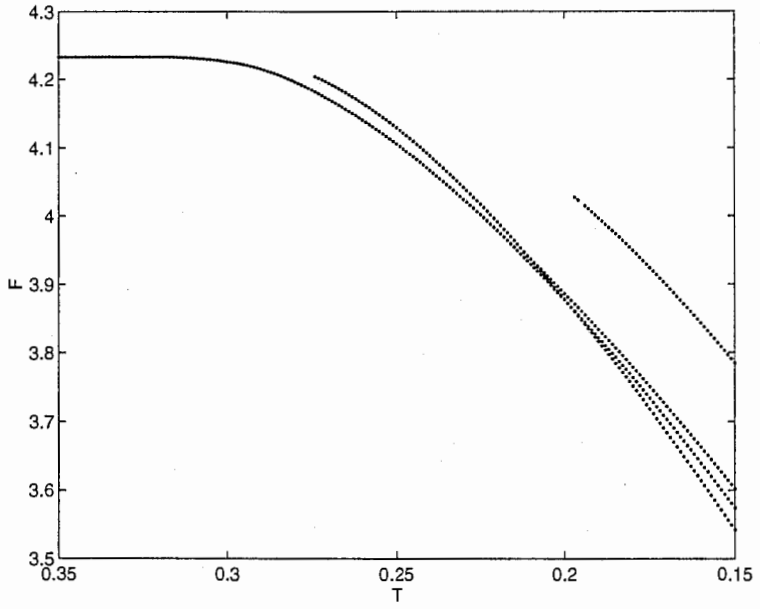

Figure 2(d)

(c) Bifurcation diagram over temperature. At each temperature 200 sets of random initial states are prepared, and $V_{1,i}$ $(i = 1, ..., 5)$ after 10000 steps are plotted. (d) The corresponding free energy diagram. A free energy crossing is observed at $T \approx 0.21$. To make the entropy term positive, this figure shows the diagram of $(E(\mathbf{V}) - T \cdot H(\mathbf{V}) + TN \log N)$, in fact.

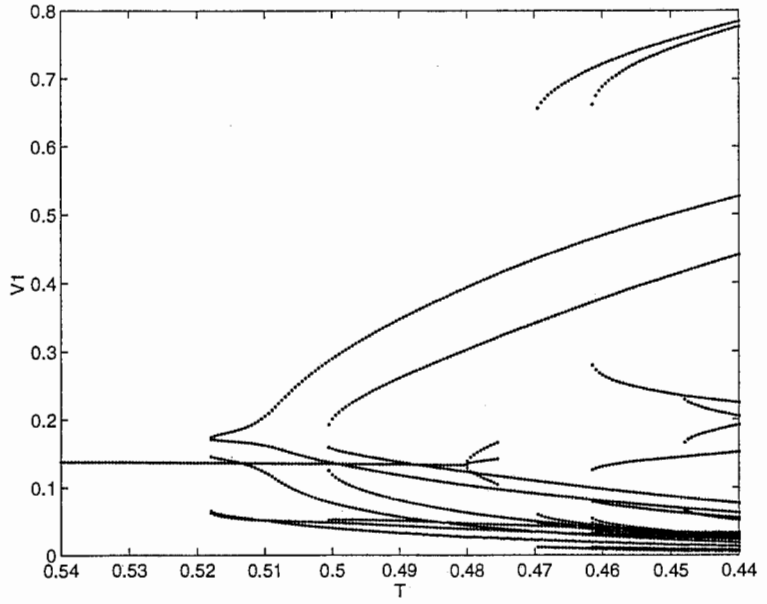

(e) Bifurcation diagram of the Ising spin MFT annealing. At each temperature 200 sets of random initial states are prepared, and $V_{1,i}$ $(i = 1, ..., 5)$ after 10000 steps are plotted. Algorithm is shown in the Appendix B.

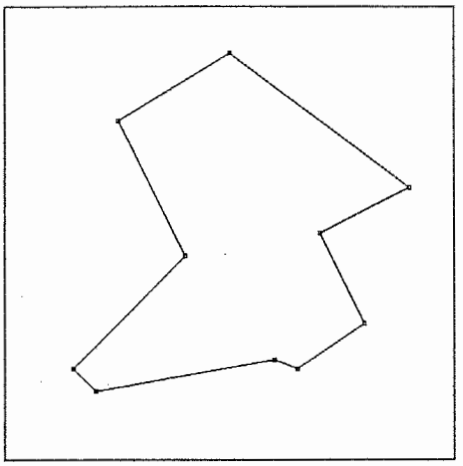

Figure 3(a)

(a) Sample 10-city problem, which is used by Hopfield and Tank (1985), and its optimal tour.

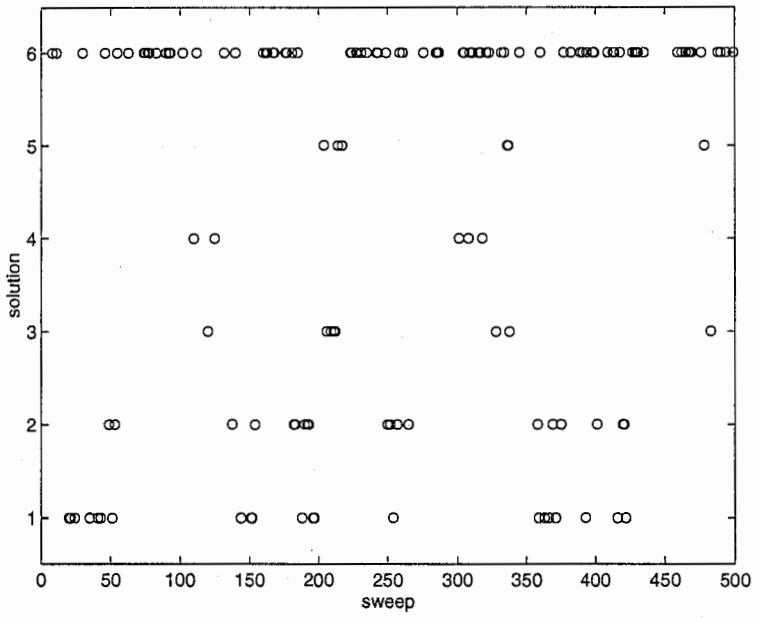

Figure 3(b)

(b) CPS process. The ordinate denotes the solution obtained at each sweep. The indices 1, 2, ..., 5, and 6 of the ordinate denote the optimal solution, the 2nd best, ..., the 5th best, and all the other valid tours, respectively. Where no circle is plotted, no valid tour is obtained at that sweep.

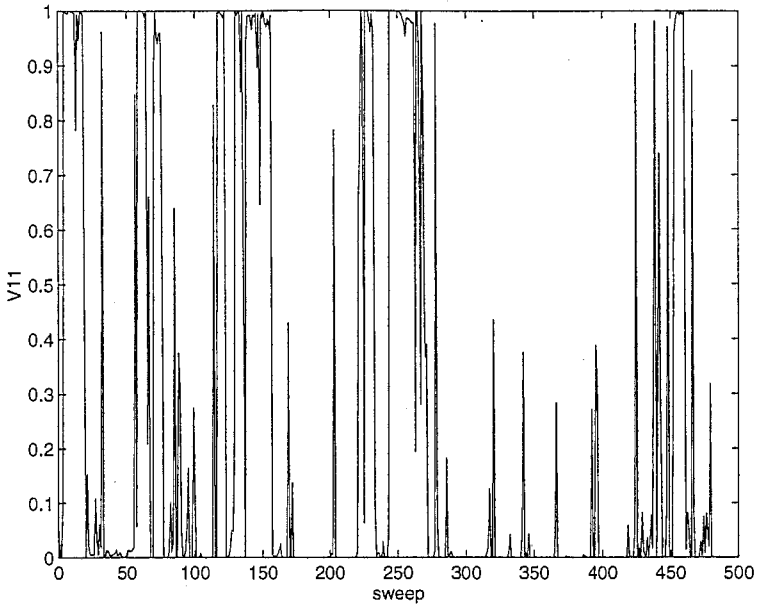

Figure 3(c)

(c) Time-series of the CPS's single variable $V_{1,1}$.

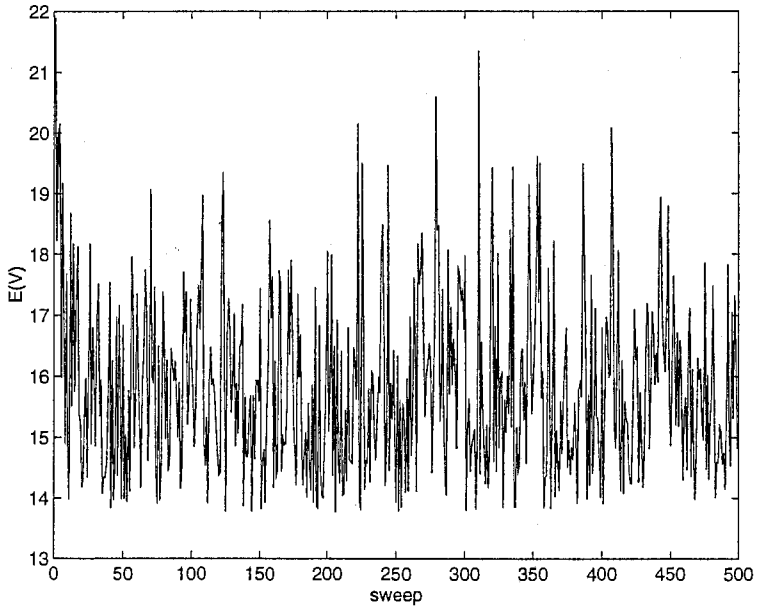

Figure 3(d)

(d) Time-series of the energy function $E(\mathbf{V})$.

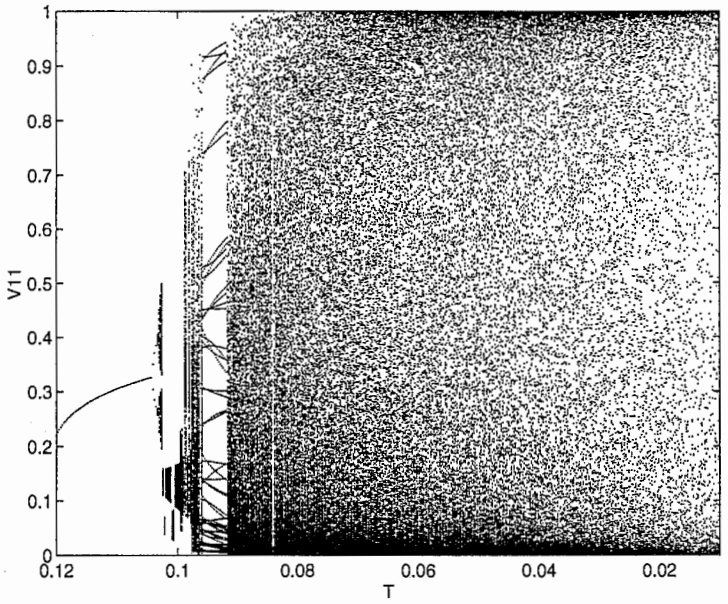

Figure 4(a)

(a) Bifurcation diagram of the fixed-order algorithm over temperature T, where values of a single variable $V_{1,1}$ at *sweep* $= 100001 \sim 100500$ are plotted at each temperature. $k = 0.7, \alpha' = 0.8$ and $\beta' = 0.0$. At each temperature, the initial state was set at $V_{a,n}(0) = 1/N +$ small-rand.

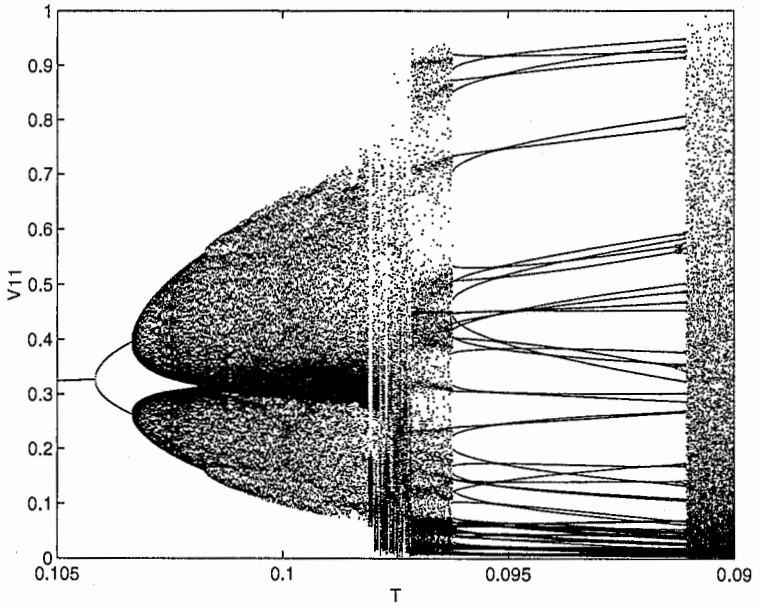

Figure 4(b)

(b) More detailed bifurcation diagram over temperature.

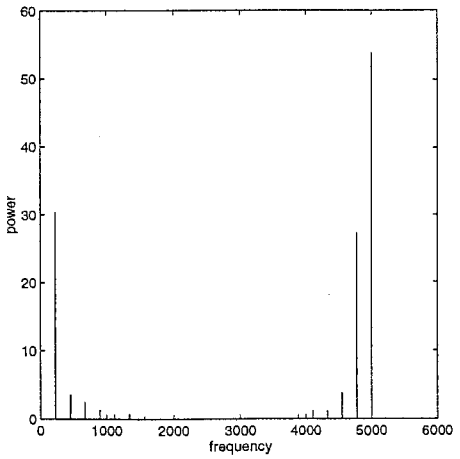

5(a1) $T = 0.1020$

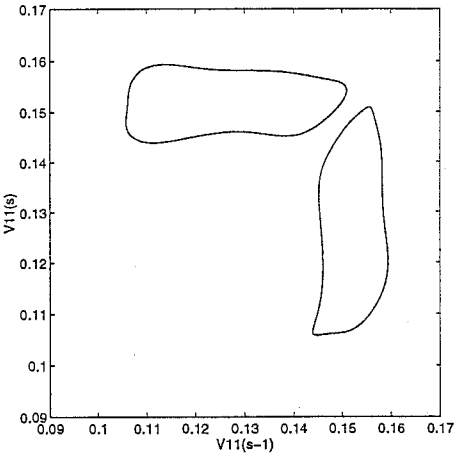

5(a2)

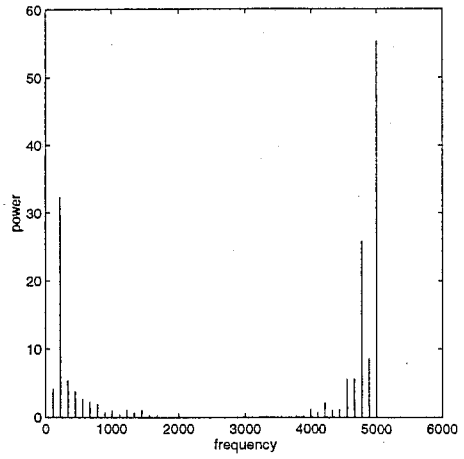

5(b1) $T = 0.1015$

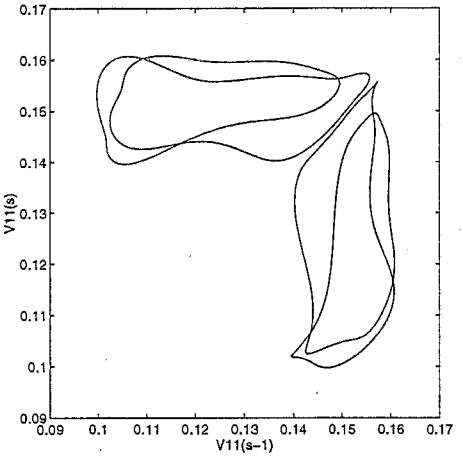

5(b2)

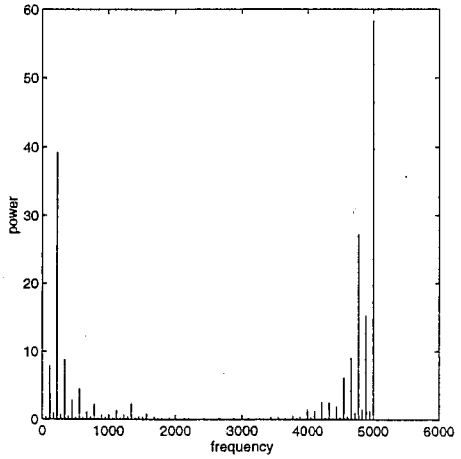

5(c1) $T = 0.1010$

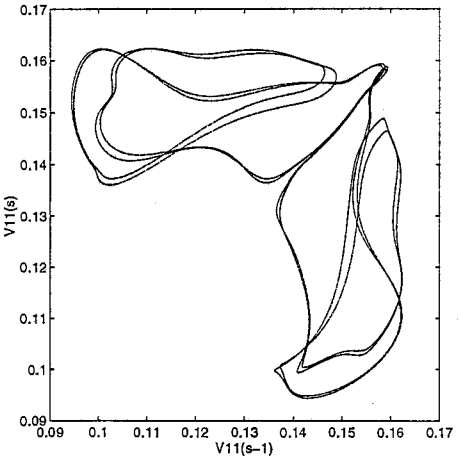

5(c2)

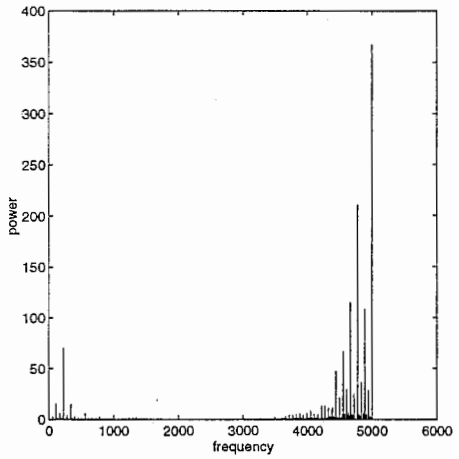

5(d1) $T = 0.1005$

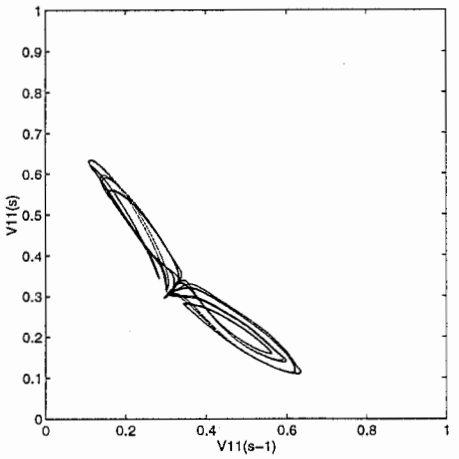

5(d2)

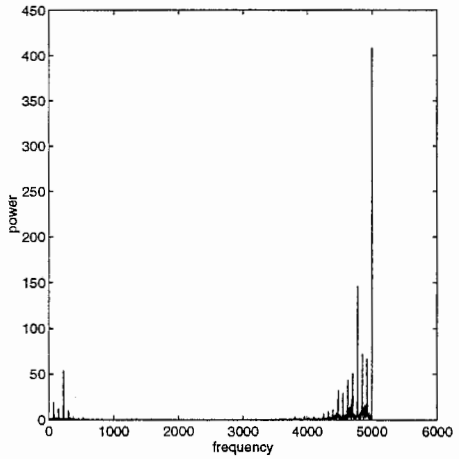

5(e1) $T = 0.1000$

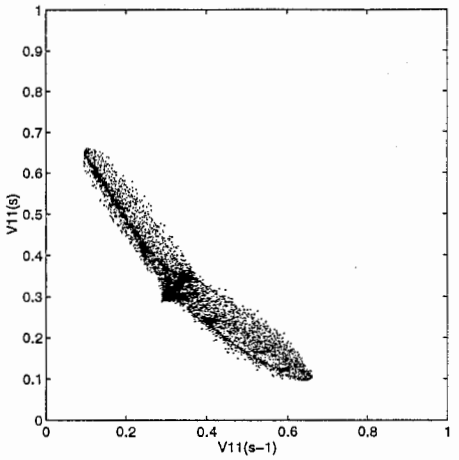

5(e2)

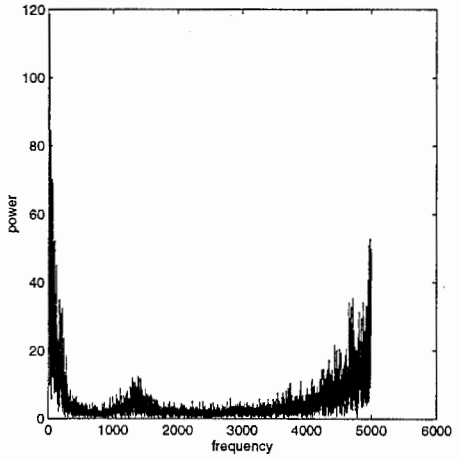

5(f1) $T = 0.0970$

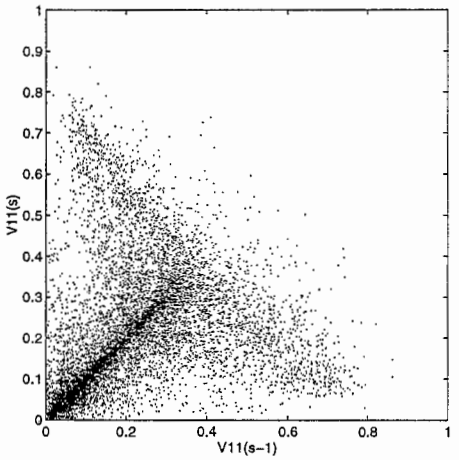

5(f2)

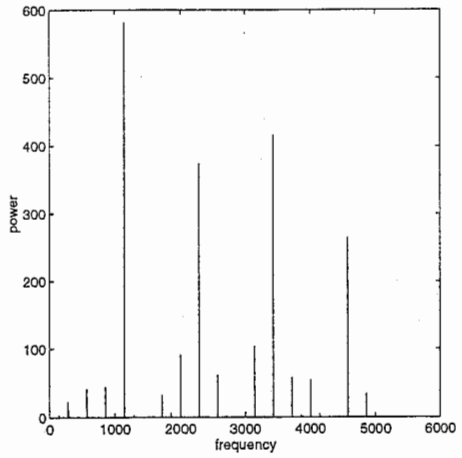

5(g1) $T = 0.0940$

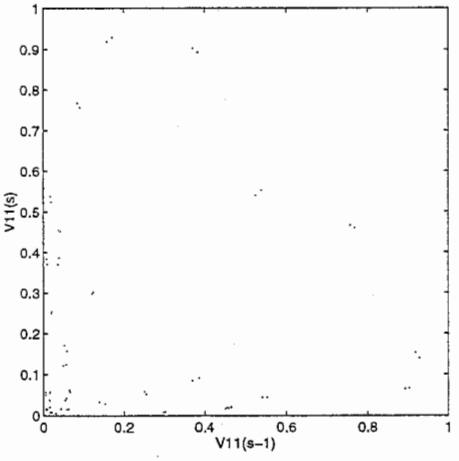

5(g2)

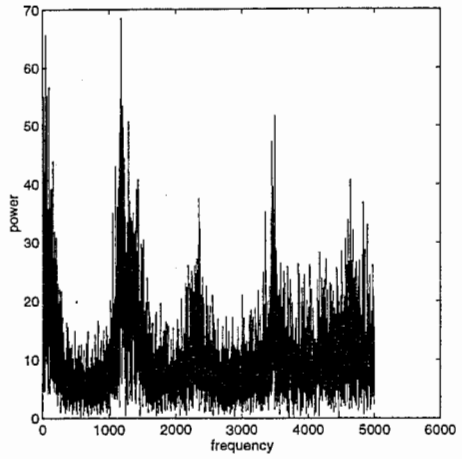

5(h1) $T = 0.0900$

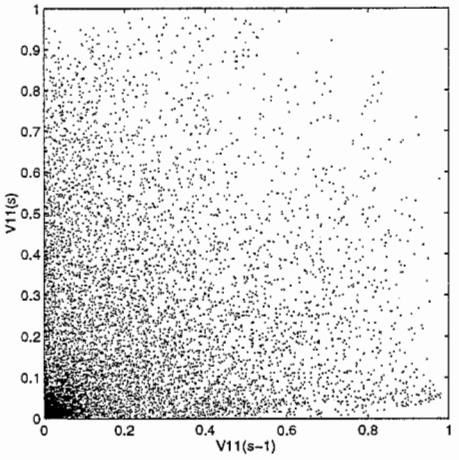

5(h2)

Figure 5

(a1) $\sim$ (h1): Frequency spectra diagrams for *sweep* $= 100001 \sim 110000$ at various temperature. (a2) $\sim$ (h2): The corresponding phase diagrams. $(V_{1,1}(s-1), V_{1,1}(s))$ $(s = 100001 \sim 110000)$ are plotted for each temperature.

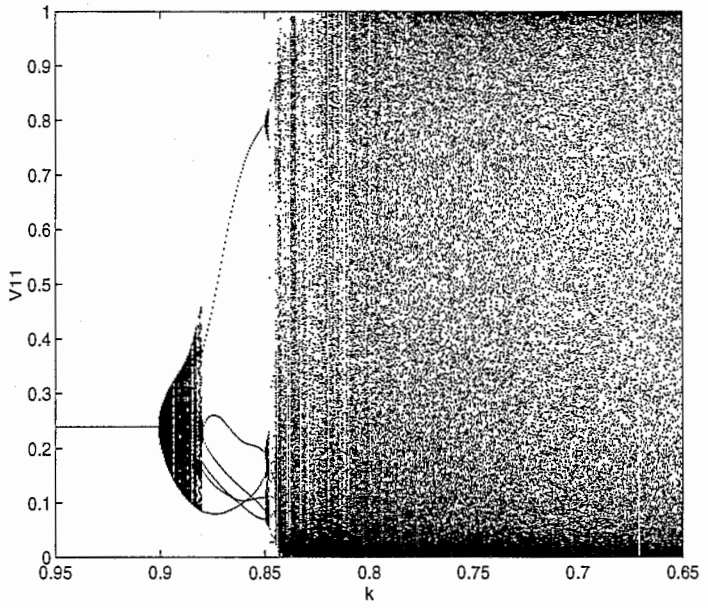

Figure 6(a)

(a) Bifurcation diagram of the fixed-order algorithm over the time-interval parameter k, where values of a single variable $V_{1,1}$ at *sweep* $= 100001 \sim 100500$ are plotted at each parameter value. $\alpha' = 2.7(1-k), \beta' = 0.0$, and $T = 0.05$. At each temperature, the initial state was set at a solution at $k = 0.95$.

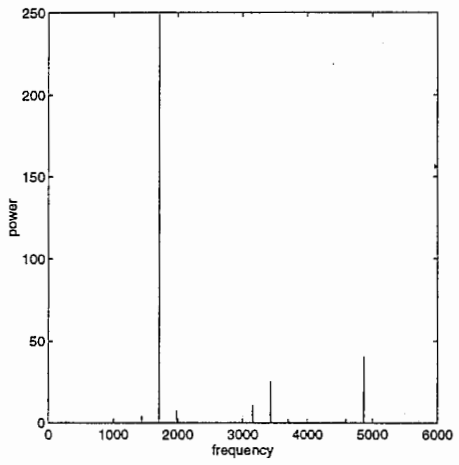

6(b)

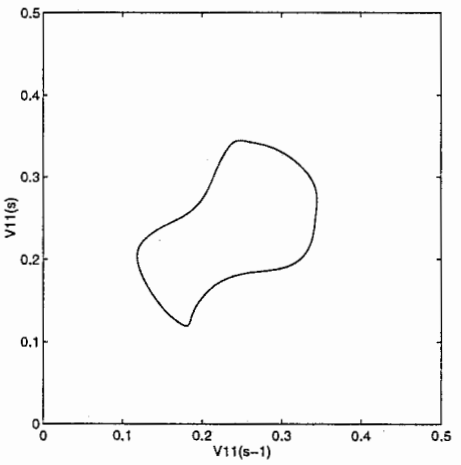

6(c)

(b) Frequency spectra diagram for *sweep* $= 100001 \sim 110000$ at $k = 0.89$. (c) Phase diagram at $k = 0.89$.

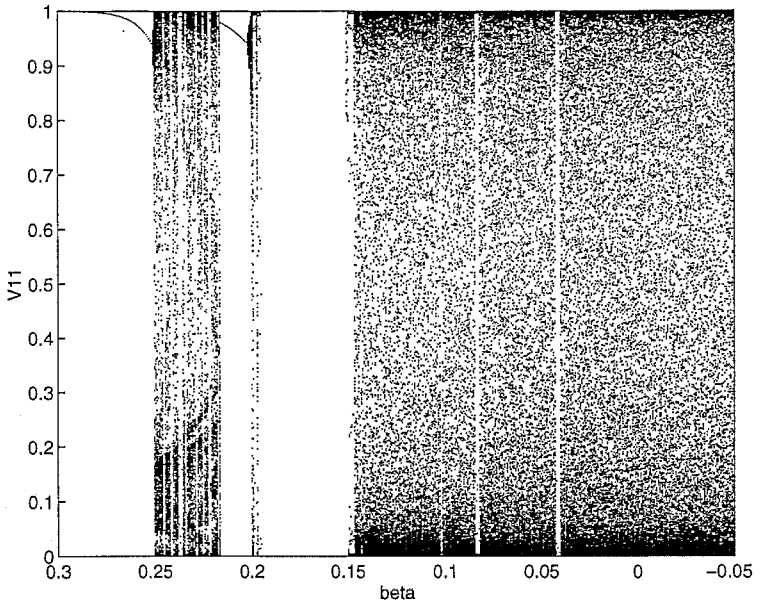

Figure 7(a)

(a) Bifurcation diagram of the fixed-order algorithm over the parameter β', where values of a single variable $V_{1,1}$ at *sweep* = 100001 $\sim$ 100500 are plotted at each parameter value. $k = 0.7, \alpha' = 0.8$, and $T = 0.05$. At each temperature, the initial state was set at $V_{a,n}(0) = 1/N +$ small-rand.

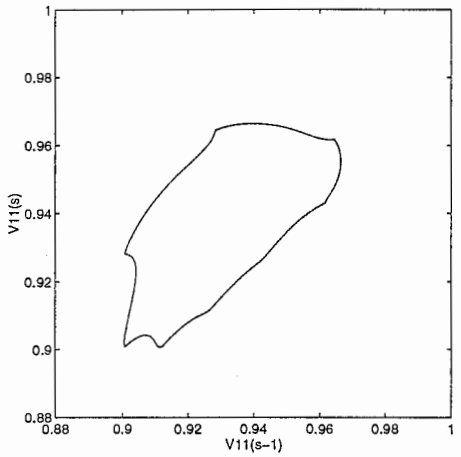

7(b) $\beta' = 0.25098$

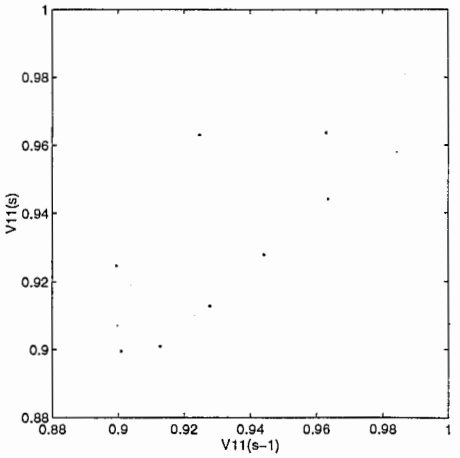

7(c) $\beta' = 0.25097$

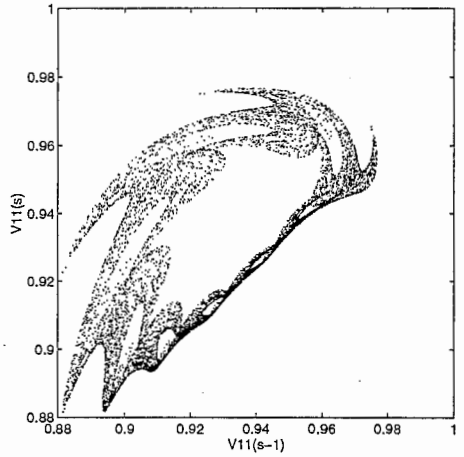

7(d) $\beta' = 0.25090$

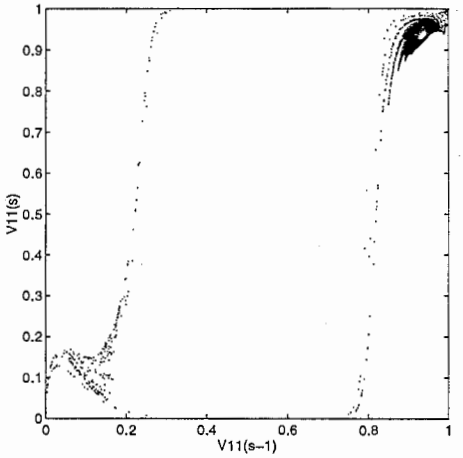

7(e) $\beta' = 0.25088$

(b) $\sim$ (e) Phase diagrams for various β' values.

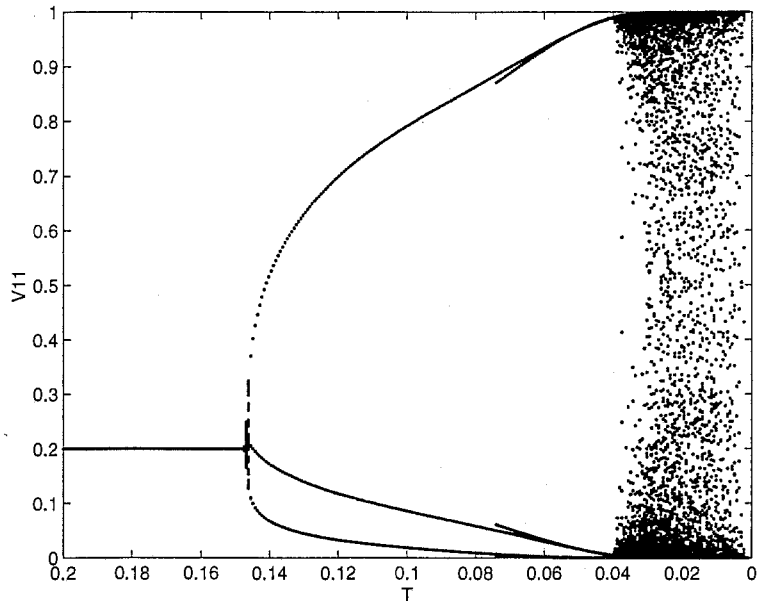

Figure 8(a)

(a) Bifurcation diagram over temperature T, where the other parameters are fixed at $k = 0.7, \alpha' = 0.22$, and $\beta' = 0.04$. At each temperature, 200 sets of initial states are prepared and each $V_{1,1}$ value for $sweep = 5001 \sim 5100$ is plotted.

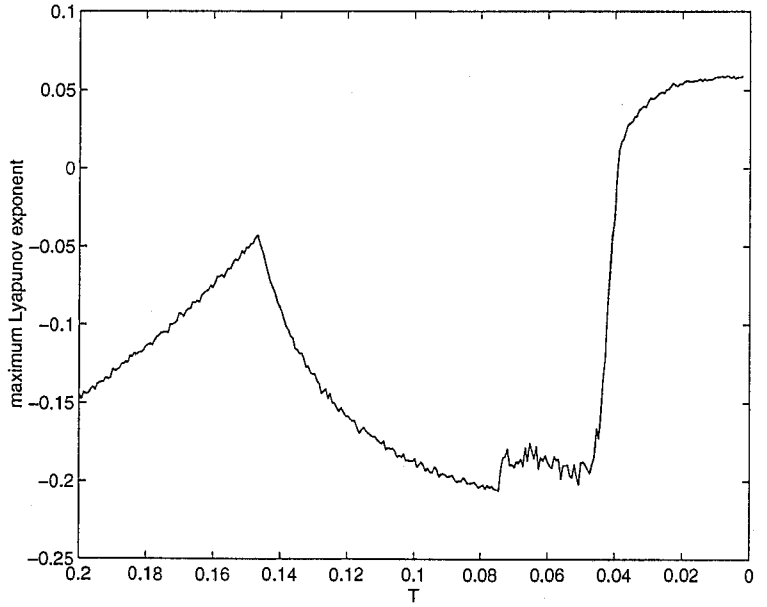

Figure 8(b)

(b) Corresponding maximum Lyapunov exponent diagram. For each temperature, exponents are averaged for 200 initial states. Each exponent is calculated for $sweep = 5001 \sim 5100$.

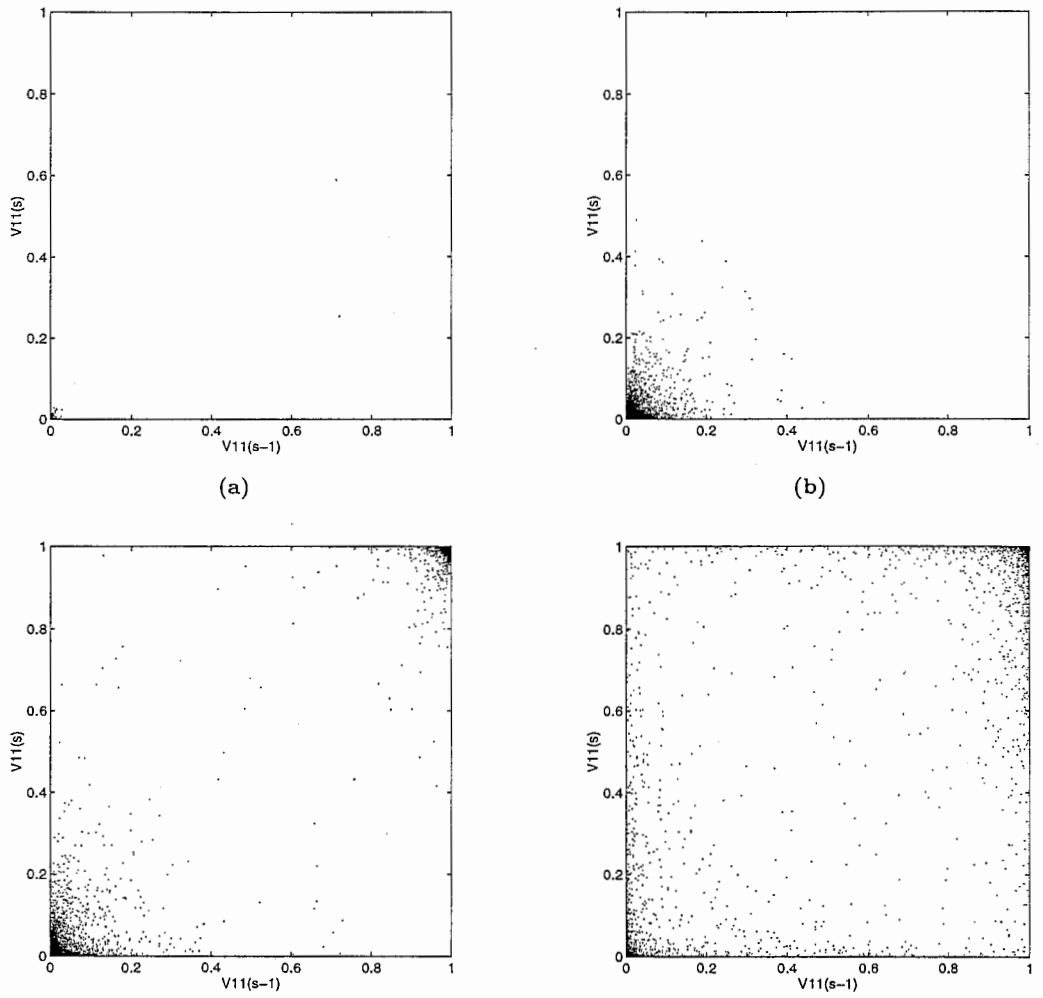

Figure 9

Phase diagrams for various temperature values. In all of the figures, $(V_{1,1}(s-1), V_{1,1}(s))$ $(s = 100001 \sim 110000)$ is plotted, where s denotes the sweep, and the initial states are set to be the same random value. (a) $T = 0.036$. (b) $T = 0.035$. (c) $T = 0.033$. (d) $T = 0.025$.

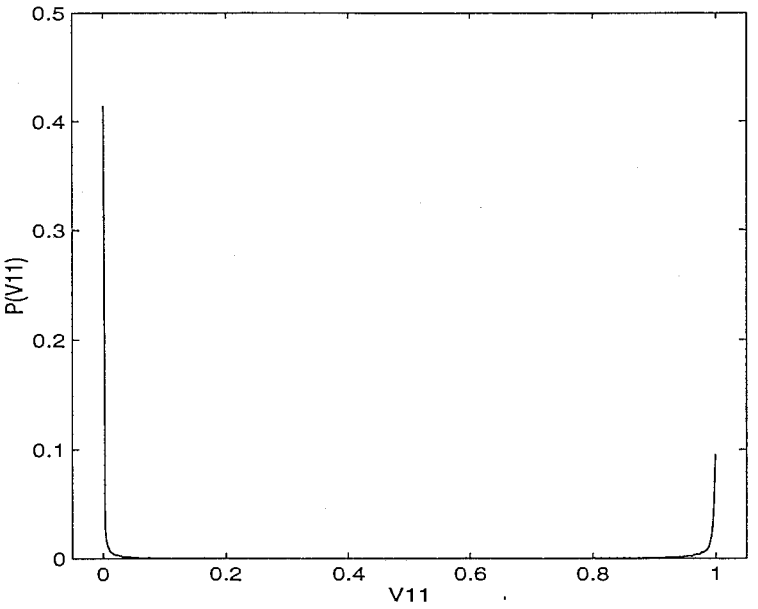

Figure 10

Value distribution of a single variable $V_{1,1}$ at $T = 0.033$. Distribution was obtained for *sweep* $= 100001 \sim 110000$.

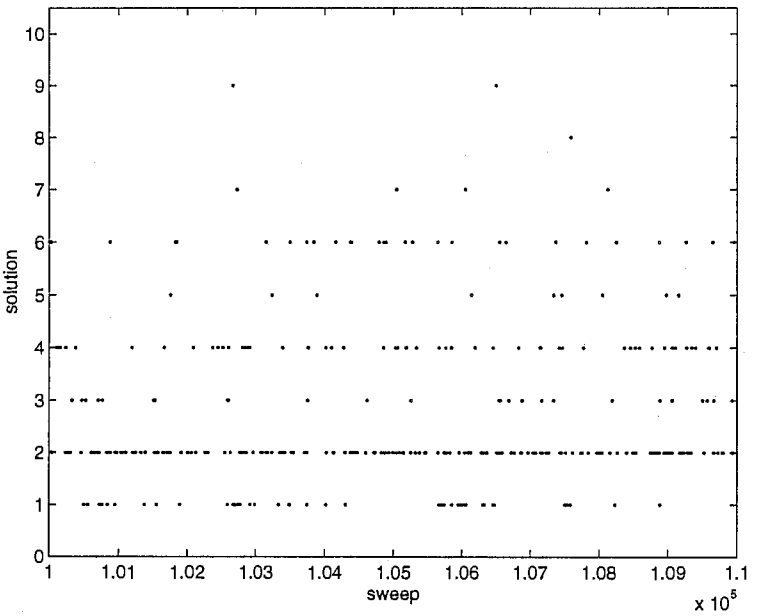

Figure 11

Obtained solutions at $T = 0.025$. Initial $\mathbf{V}$ is set randomly and solutions for *sweep* $=$ $100001 \sim 110000$ are plotted. The indices 1, 2, ..., 10 of the ordinate denote the optimal solution, the 2nd best, ..., the 10th best, respectively. When no point is plotted, no valid tour is obtained at that sweep.

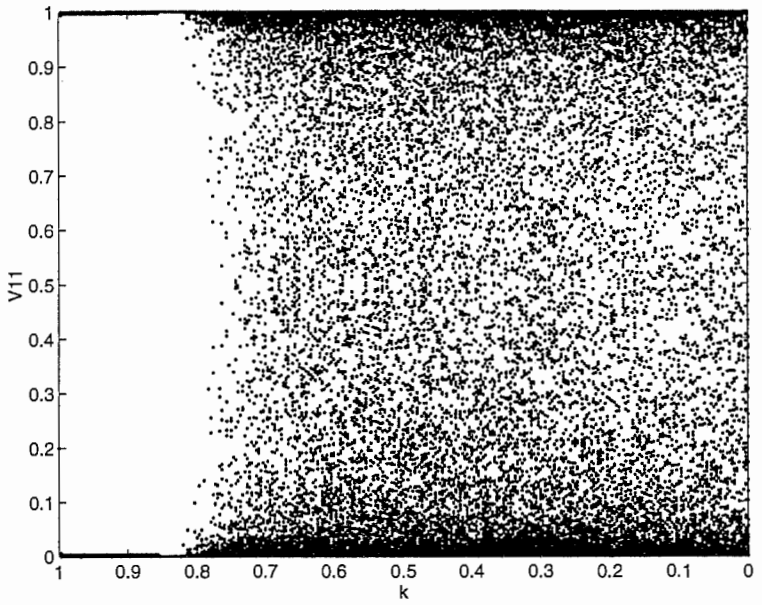

Figure 12(a)

(a) Bifurcation diagram over the time interval parameter k. For each k, 200 random initial states are prepared and each $V_{1,1}$ value for $sweep = 5001 \sim 5100$ is plotted.

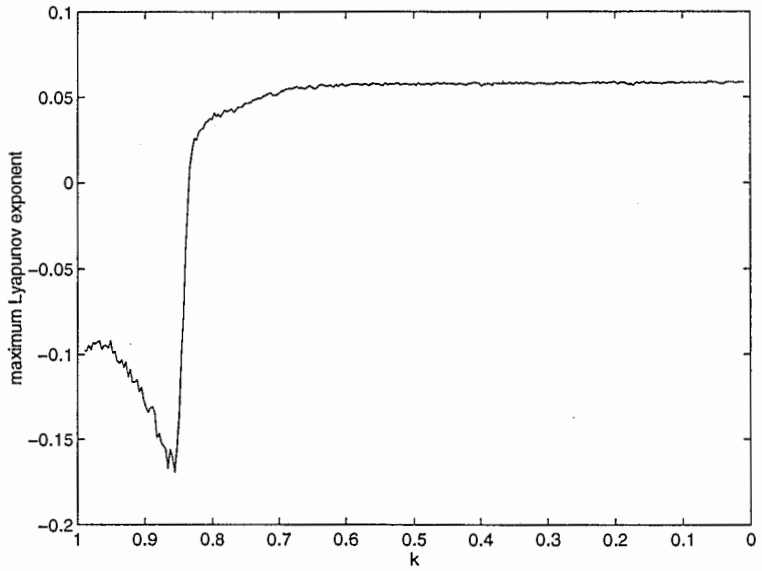

Figure 12(b)

(b) Corresponding maximum Lyapunov exponent diagram. For each k, exponents are averaged for 200 initial states. Each exponent is calculated in $sweep = 5001 \sim 5100$.

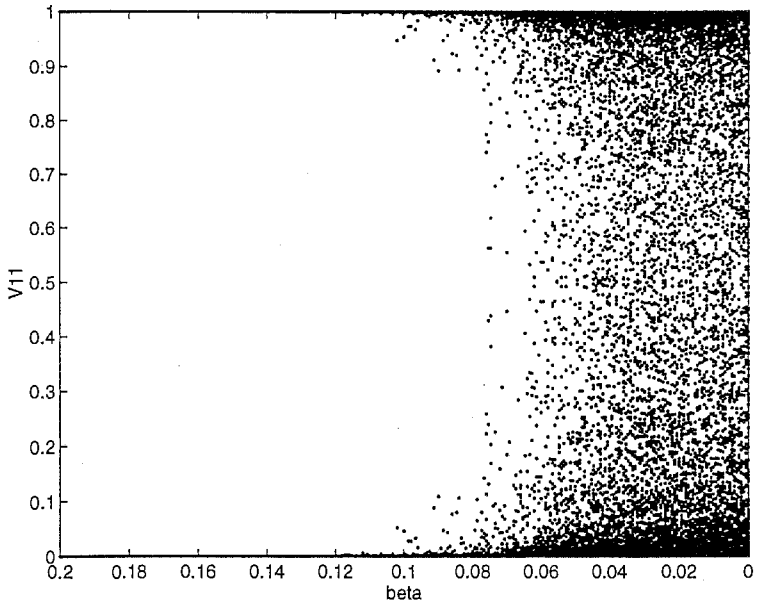

Figure 13(a)

(a) Bifurcation diagram over the self-loop parameter β'. For each β', 200 random initial states are prepared and each $V_{1,1}$ value for $sweep = 5001 \sim 5100$ is plotted.

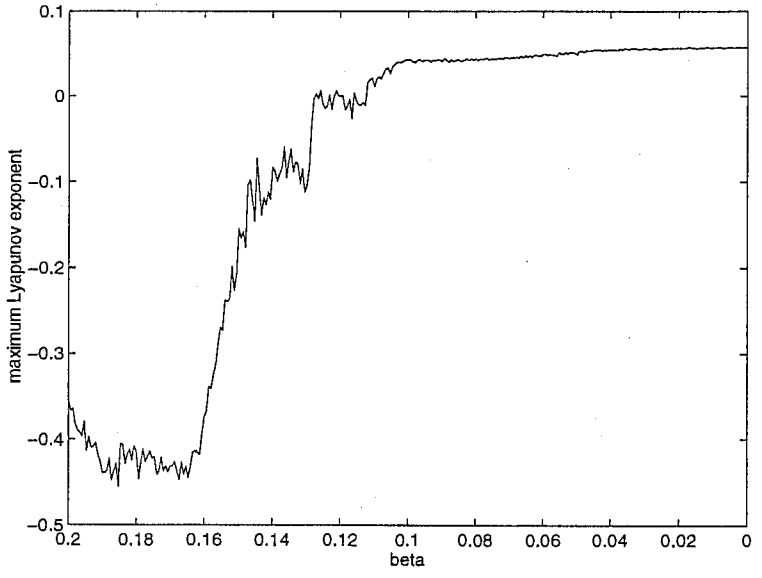

Figure 13(b)

(b) Corresponding maximum Lyapunov exponent diagram. For each β', exponents are averaged for 200 initial states. Each exponent is calculated in $sweep = 5001 \sim 5100$.

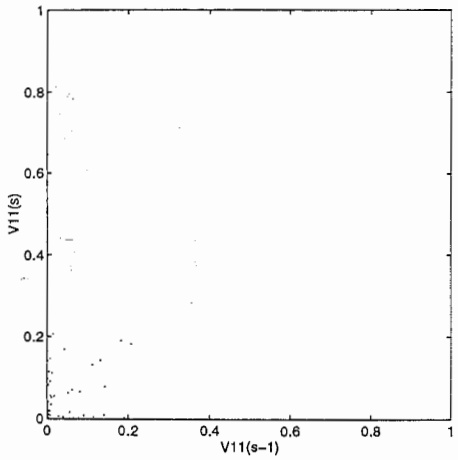

Figure 12(c)

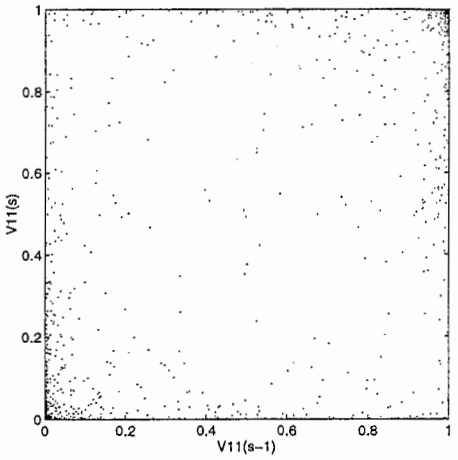

Figure 12(d)

Phase diagrams of a single variable $V_{1,1}$. In both figures, $(V_{1,1}(s-1), V_{1,1}(s))$ $(s = 100001 \sim 110000)$ is plotted, where s denotes the sweep, and the initial states are set to be the same random value. (c) $k = 0.78$. (d) $k = 0.73$.

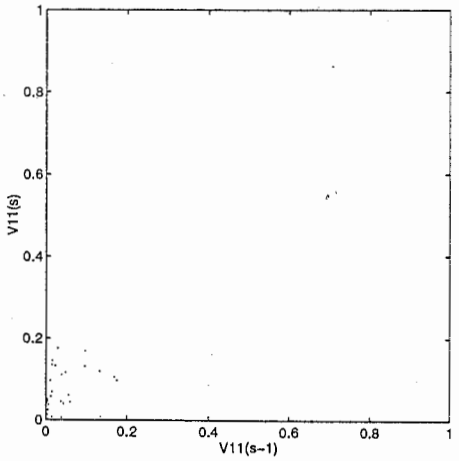

Figure 13(c)

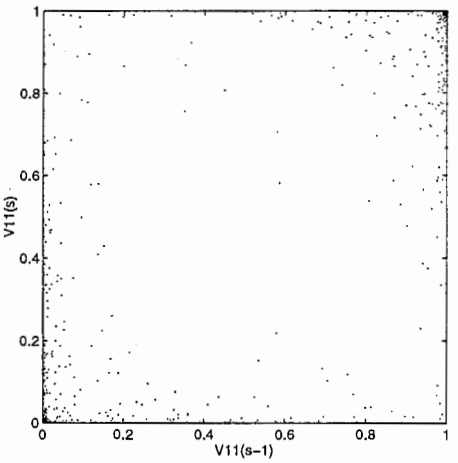

Figure 13(d)

Phase diagrams of a single variable $V_{1,1}$. In both figures, $(V_{1,1}(s-1), V_{1,1}(s))$ $(s = 100001 \sim 110000)$ is plotted, where s denotes the sweep, and the initial states are set to be the same random value. (c) $\beta' = 0.08$. (d) $\beta' = 0.06$.